ORGANIC CLATHRATES: STRUCTURE AND REACTIVITY

Author:
KANYISA L. NOHAKO

A thesis submitted to the Cape Peninsula University of Technology in fulfilment of the requirements for the

MASTERS DEGREE IN TECHNOLOGY
(CHEMISTRY)

Department of Chemistry

October 2009

ACKNOWLEDGEMENTS

I would like to thank:

- My supervisor, Dr Ayesha Jacobs for her patience and understanding, and for assisting me throughout my project.
- Prof. Luigi Nassimbeni for his guidance and courage.
- The Crystal Engineering unit for helping me when I needed it.
- My family and friends for their support.
- Mr Mei for all the help.
- Last but not least the Cape Peninsula University of Technology and National Research Foundation (Pretoria) for funding.

PUBLICATIONS AND CONFERENCES

Parts of this thesis have been presented at the following conferences:

- Poster entitled: Solid guests included by 9-(4-methoxyphenyl)-9H-xanthen-9-ol Ayesha Jacobs, Kanyisa L. Nohako, Luigi R. Nassimbeni, Gaëlle Ramon, Jana H. Taljaard. 39th South African Chemical Institute Conference (39th SACI), Stellenbosch, South Africa, 30 November – 5 December 2008.
- Poster entitled: Solid guests included by 9-(4-methoxyphenyl)-9H-xanthen-9-ol Ayesha Jacobs, Kanyisa L Nohako, Luigi R. Nassimbeni, Gaëlle Ramon, Jana H. Taljaard. Celebrating Research Seminar, Cape Peninsula University of Technology Bellville Campus, South Africa, 28 November 2008.

Parts of this thesis have been published:

- Enclathration by a xanthenol host *via* solid – solid reactions: Structure and Kinetics, Ayesha Jacobs, Luigi R. Nassimbeni, Kanyisa L. Nohako, Gaëlle Ramon, Jana H. Taljaard, *New Journal of Chemistry*, **2009**, 33, 1960-1964.

AUTHOR: Kanyisa L. Nohako

TITLE: Organic clathrates: structure and reactivity

DATE: October 2009

ABSTRACT

The host compound 9-(4-methoxyphenyl)-9H-xanthen-9-ol (A1) forms inclusion compounds with the solid guests 1-naphthylamine (NAPH), 8-hydroxyquinoline (HQ), acridine (ACRI), 1,4 – diazabicyclo[2.2.2]octane (DABCO) and a liquid guest benzaldehyde (BENZAL). All four structures A1·½NAPH, A1·½HQ A1·ACRI and A1·½DABCO were successfully solved in the triclinic space group $P\bar{1}$. The structure of A1·½BENZAL was successfully solved in the monoclinic space group $P2_1/n$. Similar packing motifs arise for the NAPH and HQ inclusion compounds where the main interaction is of the form (Host)–OH···O–(Host). Both the DABCO and the ACRI guests hydrogen bond to the host molecule. The host: guest ratios for A1·ACRI, A1·½NAPH, A1·½DABCO and A1·½HQ were found using nuclear magnetic resonance (NMR) spectroscopy. The host:guest ratio for A1·½BENZAL was found using thermogravimetric analysis. Enthalpy changes of the inclusion compounds were monitored using differential scanning calorimetry (DSC). Kinetics of desolvation for A1·½BENZAL were conducted using a non – isothermal method where we have obtained an activation energy range of 74 k J mol^{-1} – 86 k J mol^{-1}. The solid – solid reaction kinetics for A1·½NAPH, A1·½HQ, A1·ACRI and A1·½DABCO were determined at room temperature using powder X-ray diffraction (PXRD). The rate constants for the solid – solid reactions were calculated as:

- A1· ½ NAPH $k = 1.85 \times 10^{-2}$ min^{-1}
- A1·½HQ $k = 2.20 \times 10^{-2}$ min^{-1}

- A1· ½ DABCO k = 2.51 x 10^{-2} min^{-1}
- A1·ACRI k = 6.10 x 10^{-3} min^{-1}

The host compound 9,9'-(ethyne-1,2-diyl)bis(fluoren-9-ol) (WEB22) forms inclusion compounds with caffeine (CAF) and methanol (MeOH). The structure for WEB22·2CAF and WEB22·MeOH were solved in the triclinic space group $P\bar{1}$ and the mixed crystal grown from a 50:50 mixture of caffeine and theophylline with methanol as a mutual solvent yielded WEB22·½CAF·MeOH and was solved in the monoclinic space group $P2_1/c$. Similar host conformations arise for the WEB22·MeOH and WEB22·½CAF·MeOH inclusion compounds whereby the hydroxyl groups on the host molecule are cis, whereas for the WEB22·2CAF the hydroxyl groups on the host are trans. All the three structures were further stabilized by π-π interactions. Enthalpy changes for the inclusion compounds WEB22·2CAF and WEB22·MeOH were monitored using differential scanning calorimetry (DSC).

TABLE OF CONTENTS — PAGE

CHAPTER 1

INTRODUCTION

INTRODUCTION

CRYSTAL ENGINEERING

> "is the design and synthesis of molecular solid-state structures with desired properties, based on an understanding and exploitation of intermolecular interactions." – G. M. J. Schmidt, Pure Appl. Chem., 1971, (27), 647[1]

The understanding of the term crystal engineering has developed rapidly since its initial use in 1971 by Schmidt [1, 2] and currently covers numerous features of solid-state intermolecular interactions, structure prediction, control and rationalization. [2] Hydrogen bonds or coordination bonds are the two main strategies exploited in crystal design. Coordination bonds were not taken into account in this study but they occur between metal centres and ligands. The main interaction prevalent in this study was hydrogen bonding. [3, 4]

Molecular recognition is found at the heart of crystal engineering, with the molecular recognition occurrence typically including an interaction involving paired hydrogen-bonding faces or an interaction between a metal and a ligand. Through comparison with the retrosynthetic proposal to organic synthesis, Desiraju invented the phrase "supramolecular synthon" to define construction blocks which are familiar to several structures and therefore can be utilised to arrange unambiguous groups in the solid state. [5] A distinctive illustration of a supramolecular synthon is represented by the carboxylic acid dimer (Fig 1(a)); [6] the alternative catemer prevents the unfavourable secondary interactions present in the dimer (Fig 1(b)).

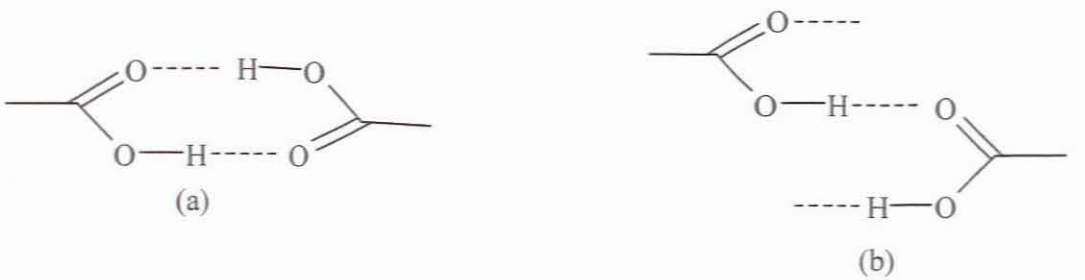

Figure 1: Supramolecular synthons based on hydrogen bonds (a) Carboxylic acid dimer, (b) alternative catemer.

SUPRAMOLECULAR CHEMISTRY

> "It is an impossible task to write a useful definition of supramolecular chemistry. The field is ever changing as it advances, and the researchers will have their own understanding and sets of terminology." – J. W Steed, Encyclopedia of Supramolecular Chemistry, 2004, 2, 1401[7]

Supramolecular chemistry can be described as "chemistry beyond the molecule" [8] and entails studying new molecular systems in which the most important feature is that the components are held together reversibly by intermolecular forces, not by covalent bonds. The area quickly developed to include molecular devices and molecular assemblies. Supramolecular chemistry intends to develop complex systems of components which interact by non-covalent intermolecular forces. [9] It permits us to study further than just one molecule and the covalent bonds needed to make that molecule.

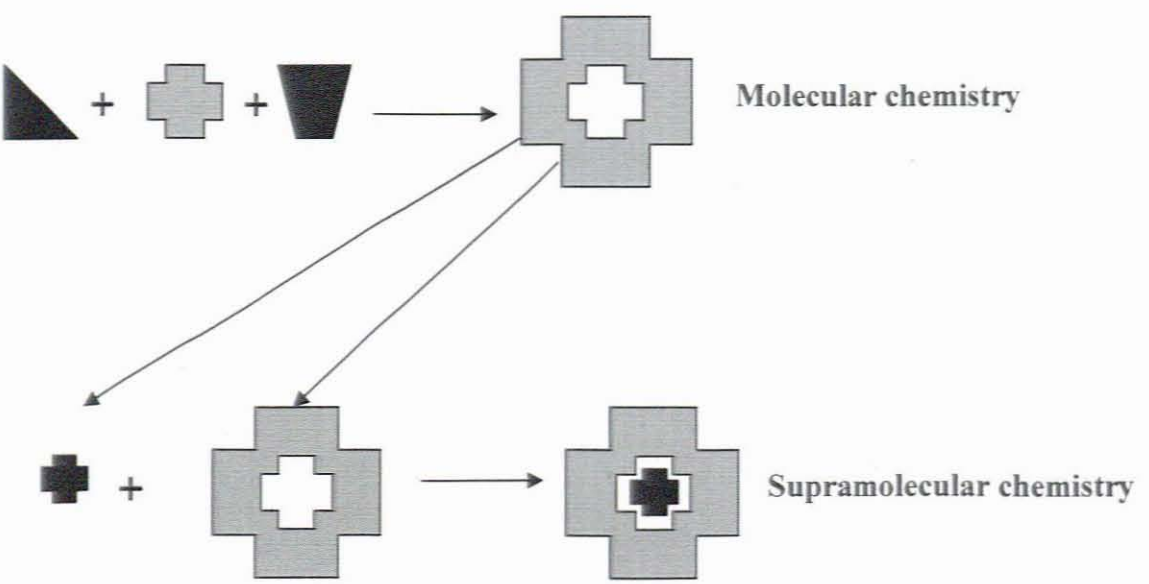

Figure 2: Link among the scope of molecular and supramolecular chemistry. [9]

WHAT IS A CO – CRYSTAL?

> "Co-crystals consist of two or more components that form a unique crystalline structure having unique properties". – Stahly, G. P.; Cryst. Growth Des.; 2007; 7; 1007. [10]

The term co-crystal is used to signify togetherness of two or more molecular components that must themselves be solids under ambient conditions, but without the insinuation that either component should keep any degree of its individual crystalline identity within the co-crystal.[9] Dunitz proposed that the togetherness refers to molecular components, so that the term co-crystal "encompasses molecular compounds, molecular complexes, solvates, inclusion compounds, channel compounds, clathrates and possibly a few other types of multi-component crystals".[11]

Throughout the text the word inclusion compound will be used for all crystalline structures involving both liquid and solid guests as stated by Dunitz above.

MOLECULAR HOST-GUEST CHEMISTRY

> "Complexes are composed of two or more molecules or ions held together in a unique structural relationship by electrostatic forces other than those of covalent bonds". – D. J. Cram, 1986 [8] (from the Encyclopedia of Supramolecular Chemistry [12])

According to Cram [8] molecular complexes are held together by a number of interactions the most common being hydrogen bonding, metal-to-ligand binding, van der Waals forces and solvent reorganisation. A high level of structural organization is usually formed using a series of binding sites and an extremely ordered molecular composite consists of no less than a single host and a single guest component. The host is characterized as an organic molecule or ion whose binding sites converge in the complex and the guest is characterized as any molecule or ion whose binding sites diverge in the complex.

SOLID-STATE HOST-GUEST CHEMISTRY

Solid-state host-guest chemistry can be traced to the discovery of the chlorine clathrate hydrate by Davy [13] in 1811 and signifies cocrystallization of two or more chemically distinct species. The nature of solid-state host-guest complexes was first exposed by Powell [14] in the 1940s using x-ray crystallography. He initiated the term "clathrate" to show a guest molecule trapped in a cavity formed by the host, formally a type of inclusion complex "in which two or more components are associated without ordinary chemical union, but through complete enclosure of one set of molecules in a suitable structure formed by another".[15] The distribution of host-guest complexes into two general categories consistent with the comparative topological association among guest and host was proposed by Vögtle and Weber.[15] Clathrands are hosts with extramolecular cavities and are only applicable to the solid state (Fig. 3(a)). Hosts with intramolecular cavities are known as cavitands (Fig 3(b)).

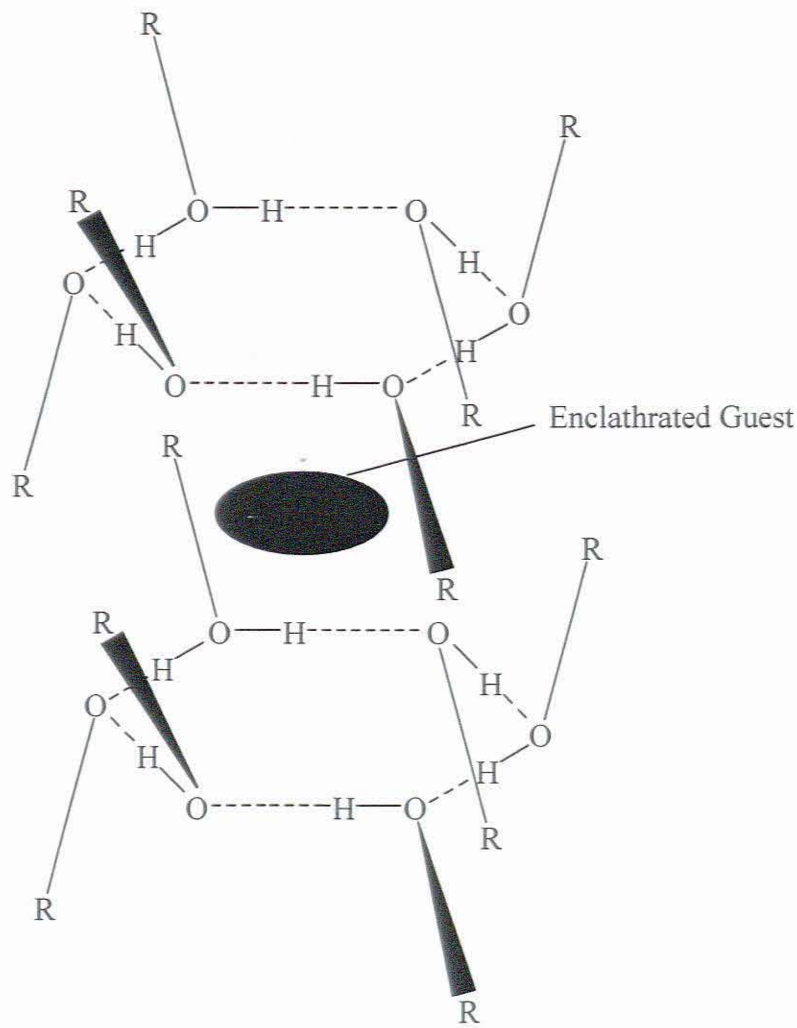

Figure 3(a): An example of a clathrand containing an enclathrated guest (black disk)

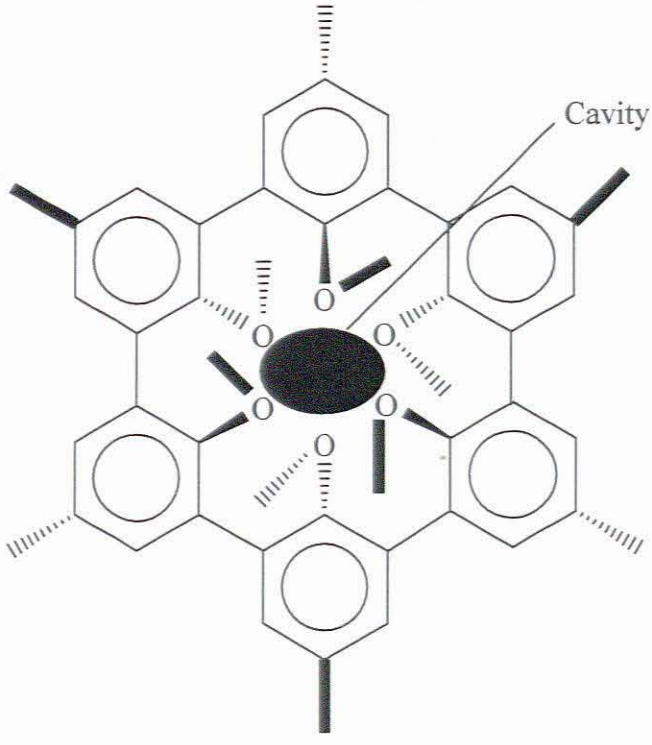

Figure 3(b): An example of a cavitand with an intramolecular cavity (black disk)

INTERMOLECULAR INTERACTIONS

Supramolecular species are held together by non-covalent interactions. The interactions are noticeably weaker than covalent interactions and can vary between 150 kJ mol^{-1} - 450 kJ mol^{-1} for single bonds.[2] A stable supramolecular complex can exist if these interactions are synergistic. The word non-covalent describes a broad series of intermolecular attractive and repulsive interactions which are summarized in Table 1.

Interaction	Strength (kJ mol^{-1})	Example
Ion-dipole	50-200	Sodium[15]crown-5
Dipole-dipole	5-50	Acetone
Hydrogen bonding	4-120	Guanine and cytosine
π-π	0-50	Benzene and graphite
Van der Waals	<5 kJ mol^{-1} but changeable depending on surface area	Argon; packing in molecular crystals

Table 1: Summary of intermolecular interactions

Ionic and Dipolar Interactions

These interactions can be divided into three groups: (i) ion-ion interactions, (ii) ion-dipole interactions and (iii) dipole-dipole interactions, which are derived from Coulombic attraction among opposed charges. Ion-ion interactions are the strongest of them all. They are non-directional in nature, meaning that the interaction can take place in any orientation. Ion-dipole and dipole-dipole interactions have orientation-dependent features demanding the alignment of two units such that the interactions are optimised. [16-17]

Hydrogen bonding

> "A hydrogen bond is an interaction that directs the association of a covalently bonded hydrogen atom with one or more other atoms, groups of atoms, or molecules into an aggregate structure that is sufficiently stable to make it convenient for the chemist to consider it as an independent chemical species". – M. C. Etter, 1990 [18] (expanded from L. Pauling, 1960 [19])

The hydrogen bond is debatably the most vital non-covalent interaction in supramolecular chemistry because of its potency and high degree of directionality. It signifies a unique category of dipole-dipole interaction involving a proton donor (D) and a proton acceptor (A). The donor group contains an electronegative atom eg. nitrogen or oxygen attached to a hydrogen atom which has a slight positive charge. The acceptor atom is also electronegative and can interact with a positively charged hydrogen atom, for example, carbonyl moieties (Fig 4).

Figure 4: (a) A carbonyl accepting a hydrogen bond from a secondary amine donor and (b) the standard way of expressing donor and acceptor atoms (D, donor atom; A, acceptor atom)

The potency, length and the character of the interaction is determined by the geometry of the hydrogen bond and the type of donor and acceptor groups. Hydrogen bond interactions can be split into three broad groups, the properties of which are listed in Table 2.

Interaction/property	Strong	Moderate	Weak
Bond length (Å)			
H·····A	1.2-1.5	1.5-2.2	2.2-3.2
D·····A	2.2-2.5	2.5-3.2	3.2-4.0
Bond angle (degrees)	175-180	130-180	90-150

Table 2: Hydrogen bond interactions and their properties (A, acceptor; D, donor)[21]

The highly directional character of hydrogen bonding interactions, in cooperation with the arrangement of hydrogen bond donors and acceptors are advantageous in supramolecular design. [20-24]

π-Interactions

Cation-π interactions and π-π interactions are the two important π-interactions which are recognized in supramolecular systems. Cation-π interactions are well known in the field of organometallic chemistry, where ethene clusters are linked to transition metal centres eg. ferrocene and Zeise's salt ($[PtCl_3(\eta^2\text{-}C_2H_4)]^-$).[25] The two types of π-π interactions are: (i) face-to-face, whereby corresponding ring-systems, approximately 3.5 Å apart are offset. The interaction is between the centre of one ring and the corner of another (Fig 5(a)), and (ii) edge-to-face, whereby a hydrogen atom from one ring interacts in a perpendicular fashion with the centre of another ring (Fig 5(b)). These π-π interactions are the result of the attraction among the negatively charged π-electron

cloud of one aromatic system and the positively charged σ-framework of the nearest molecule. [25- 26]

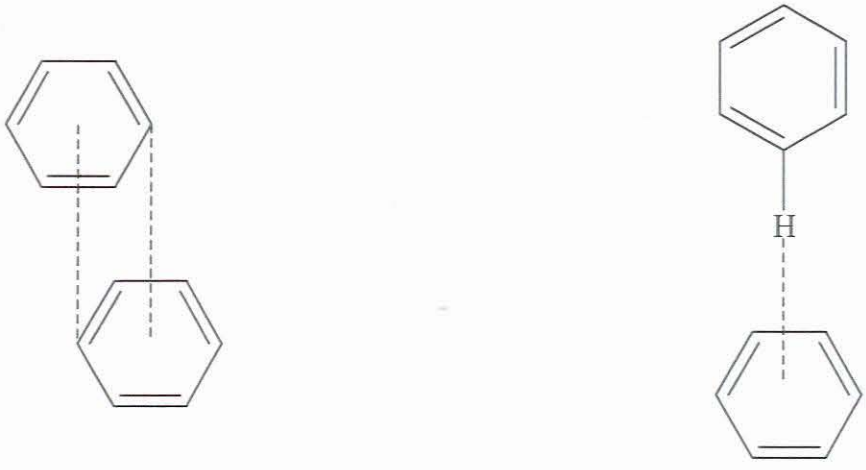

(a) (b)

Figure 5: The two forms of π-π interactions: (a) face-to-face; (b) edge-to-face

Van der Waals Interactions

Van der Waals interactions are defined as dispersive intermolecular forces. [27] They are due to the fluctuations of the electron cloud between species that are in close proximity to one another. These forces are non-directional and have a limited impact on supramolecular design. Their strength is dependent on the polarisability of the molecule and is most significant in compounds where small organic guests are incorporated in crystal lattices or molecular cavities. [28-29]

SOLID-SOLID REACTIONS

Solid-solid reactions are "solvent free" reactions carried out in the solid state mainly through grinding experiments. It is hard to control these reactions because of the grinding time and pressure exerted by the operator giving rise to changes in temperature. Schmidt [30] was the first to study this type of reaction. Braga and Grepioni used $[Fe(\eta^5\text{-}C_4H_5\text{-}1\text{-}C_5H_4N)_2]$ to prepare a series of mixed-metal compounds with different transition metal salts via the co-grinding method.[31-35] Toda [36], Rothenberg [37] and their co-workers confirmed that solid state reactions can proceed to completion more efficiently than in solution.

REACTIVITY

Reactivity is the rate at which a chemical substance is likely to undergo a chemical reaction in time. The reactivity of pure compounds depends on the physical properties of the sample. Grinding a sample to a powder enhances its reactivity. The reactivity of impure compounds is affected by the inclusion of contaminants. The crystalline form can also have an effect on reactivity.

ABOUT THIS STUDY

The aim of this study was to further investigate the ability of 9-(4-methoxyphenyl)-9H-xanthen-9-ol (A1) to include solid [38] and liquid [39] guests. Various solid guests were included by A1, namely: acridine, 1, 4-diazabicyclo [2.2.2] octane (TEDA), 1-naphthylamine and 8-hydroxyquinoline. The structures were determined and the kinetics of the solid-solid reactions investigated by powder x-ray diffraction. The structure of A1 with the liquid guest benzaldehyde was also determined and the kinetics of desolvation investigated. Nuclear magnetic resonance spectroscopy was used to determine the host: guest ratio of the inclusion compounds formed.

The study was extended to the diol host, 9,9'-(ethyne-1,2-diyl)bis(fluoren-9-ol) (WEB22). The selectivity of WEB22 for caffeine and theophylline as guests was studied using methanol as a co-solvent.

REFERENCES

1. Schmidt, G. M. J. *Pure Appl. Chem.* **1971,** 27, 647.
2. Steed, J. W.; Atwood, J. L. Supramolecular Chemistry, John Wiley & Sons, Ltd., **2000**.
3. Aakeröy, C. B.; Beatty, A. M. *Aust. J. Chem.* **2001,** 54 (7), 409 - 421.
4. Meléndez, R. E.; Hamilton, A. D. *Top. Curr. Chem.* **1998,** 198, 97 - 129.
5. Desiraju, G. R. *Angew. Chem. Int. Ed. Engl.* **1995,** 34 (21), 2311-2327.
6. Allen, F. H.; Motherwell, W. D. S.; Raithby, P. R.; Shields, G. P.; Taylor, R. *New, J. Chem.* **1999**, 23 (1), 25-34.
7. Steed, J. W. *Encyclopedia of Supramolecular Chemistry*, **2004**, 2, 1401.
8. Cram, D. J. *Angew. Chem. Int. Ed. Engl.* **1986,** 25, 1039.
9. Lehn, J. M. *Angew. Chem. Int. Ed. Engl.* (Nobel lecture) **1988,** 27, 89 - 112.
10. Stahly, G. P. *Cryst. Growth Des.* **2007,** 7, 1007.
11. Dunitz, J. D. *CrystEngComm.* **2003,** 5, 506
12. Atwood, J. L.; Steed, J. W. *Encyclopedia of Supramolecular Chemistry*. Vol. 1-2. eds. Marcel Dekker, Inc. New York. **2004**.
13. Davy, H. *Philos. Trans. R. Soc.* London. **1811,** 101, 1.
14. Powell, H. J. *J. Chem. Soc.* **1961**, 73, 5691.
15. Weber, E. *Top. Curr. Chem.* **1987**, 140, 2-20.
16. Steed, J. W. *Encyclopedia of Supramolecular Chemistry*. **2004**, 2, 1403-1404.
17. Anslyn, E. V.; Dougherty, D. A. *University Science Books*. Sausalito. CA. USA. **2006**, 162-168.
18. Etter, M. C. *Acc. Chem. Res.* **1990**, 23, 120.
19. Pauling, U. L. 3rd Ed; *Cornell University Press*. Ithaca. NY. **1960**, 6.
20. Braga, D. *Encyclopedia of Supramolecular Chemistry*. 357.

21. Jeffery, G. A. *Oxford University Press*. Oxford. UK. **1997**.

22. Desiraju, G. R. *Elsevier: Amsterdam*. **1989,** Ch. 5.

23. Gilli, P.; Bertolasi, V.; Ferreti, V.; Gilli, G. *Acta Cryst*, **1995**, 351, 1004.

24. Gilli, P.; Bertolasi, V.; Ferreti, V.; Gilli, G. *Am. Chem. Soc*. **1994**, 116, 909.

25. Etter, M. C. *J. Phys. Chem*. **1991**, 95, 4601- 4610.

26. Ma, J. C.; Dougherty, D. A.*Chem. Rev*. **1997**, 97, 1303-1324.

27. Hunter, C. A.; Lawson, K. R. J. Perkins, C. J. Urch; *J. Chem. Soc. Perkin Trans*. 2. **2001**, 651-669.

28. Steed, J. W.; Atwood, J. L. *Supramolecular Chemistry.* John Wiley & Sons. Chichester. **2000.**

29. Schneider, H. J. *Encyclopedia of Supramolecular Chemistry*. Vol. 2, J. W. Steed, W. and Atwood, J. L. (Eds), *Marcel Dekker*. New York. NY. USA. **2004**, 1550-1556.

30. Schmidt, G. M. J. *Pure Appl. Chem*. **1971**, 27, 647.

31. Braga, D.; Grepioni, F. *Coord. Chem. Rev*. **1999**, 183, 19- 41.

32. Braga, D.; Grepioni, F. *J. Chem. Soc. Dalton Trans.* **1999**, 1.

33. Braga, D.; Grepioni, F. *Chem. Soc. Rev*. **2000**, 29, 229- 238.

34. Braga, D.; Grepioni, F. *Chem. Commun*. **2005**, 3, 635.

35. Braga, D.; Giaffreda, S. L.; Grepioni, F.; Pettersen, A.; Maini, L.; Maini, M.; Curzi, M.; Polito, M. *Dalton Trans*. **2006**, 1249- 1263.

36. Toda, F.; Takumi H.; Akeni M. *J. Am. Chem. Soc*. Chem. Commun. **1990**, 1271.

37. Rothenberg, G.; Downie, A. P.; Raston, C. L.; Scott, J. L. *J. Am. Chem. Soc*. **2001**, 123, 8701.

38. Curtis, E.; Nassimbeni, L. R.; Su, H.; Taljaard, J. H. *Cryst. Growth Des.* **2006**, 6, 12, 2716 – 2719.

39. Faleni, N.; Jacobs, A.; Nassimbeni, L. R.; Taljaard, J. H. *Cryst. Growth Des.* **2007**, 7, 6, 1003 – 1006.

CHAPTER 2

EXPERIMENTAL MATERIALS AND METHODS

EXPERIMENTAL MATERIALS AND METHODS

HOST COMPOUNDS

The host compound 9-(4-methoxyphenyl)-9H-xanthen-9-ol henceforth referred to as A1 and the host compound 9,9'-(ethyne-1,2-diyl)bis(fluoren-9-ol) hereafter referred to as WEB22 are organic host compounds which conform to Weber's rule for host design. They are bulky, rigid and have hydroxyl moieties that can act as hydrogen-bond donors. A1 has an ether oxygen which is a potential hydrogen-bond acceptor.

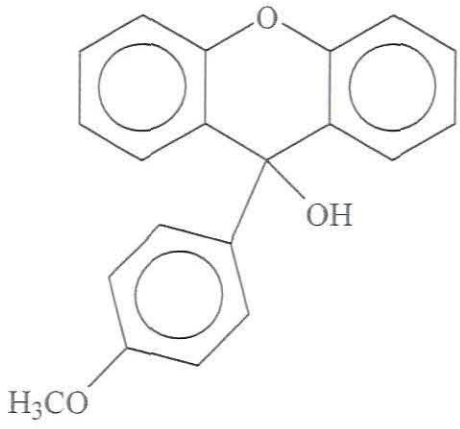

Scheme 1 : 9-(4-methoxyphenyl)-9H-xanthen-9-ol

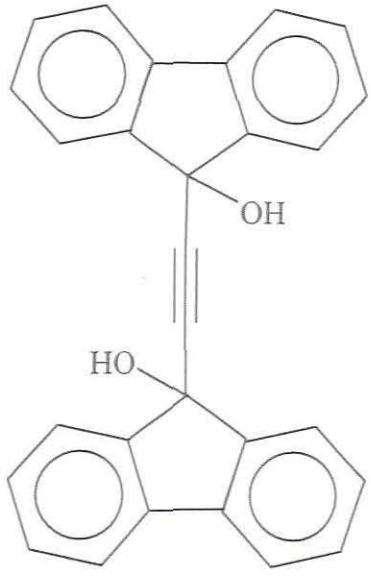

Scheme 2: 9,9'-(ethyne-1,2-diyl)bis(fluoren-9-ol)

GUEST COMPOUNDS

8-Hydroxyquinoline (HQ), acridine (ACRI) and 1,4-diazabicyclo[2.2.2]octane (DABCO) were supplied by Merck & Co.; 1-Naphthylamine (NAPH) was supplied by BDH Chemicals Ltd England; benzaldehyde (BENZAL) was supplied by Merck & Co; caffeine (CAF) and theophylline (THEO) were supplied by SIGMA Chemical Co. All the guests were used as they were.

Guest Compounds	**Molecular Formula**	**Mol wt. (g mol^{-1})**	**Bp (°C)**	**Mp (°C)**
Acridine	$C_{13}H_9N$	179.2		107
Benzaldehyde	C_6H_5CHO	106.1	179	
Caffeine	$C_8H_{10}N_4O_2$	194.2		238
1,4-Diazabicyclo[2.2.2]octane	$C_6H_{12}N_2$	112.2		156
8-Hydroxyquinoline	C_9H_7NO	145.2		76
1-Naphthylamine	$C_{10}H_9N$	143.2		50
Theophylline	$C_7H_8N_4O_2$	180.0		271

Table 3: Physical properties of the guest compounds studied

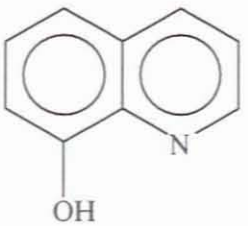

HQ

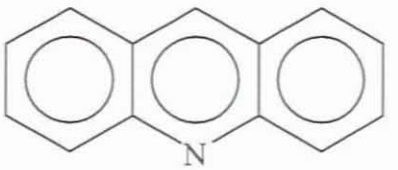

ACRI

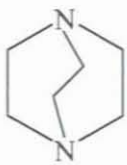

DABCO

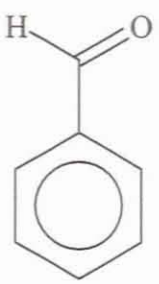

BENZAL

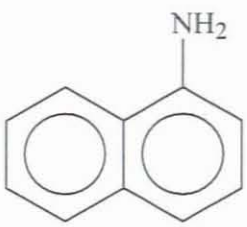

NAPH

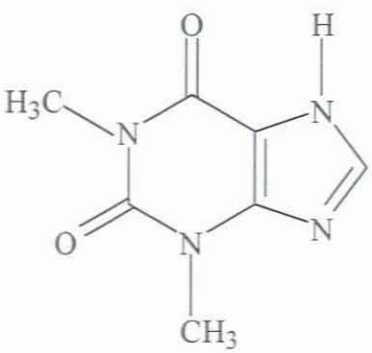

THEO

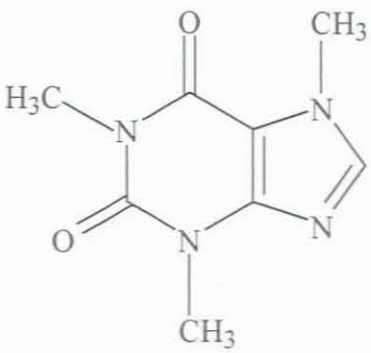

CAF

Scheme 3: Guest compounds

CRYSTAL GROWTH

The inclusion compounds were prepared by dissolving the host in an excess of its respective heated guest at 343 K by gentle stirring on a hot plate. The solution was covered with pierced Parafilm and left to crystallise by slow evaporation at room temperature. For solid guests an appropriate intermediate solvent that does not form an inclusion compound with the relevant host was used for dissolution. Full details for each compound are given in the respective chapters.

THERMAL ANALYSIS

Differential Scanning Calorimetry (DSC)

In a DSC analysis, the enthalpy changes are measured while a sample is heated at a constant rate. The changes can be accredited to desolvation, phase transformations, melting and other thermal proceedings that take place as the inclusion compound is heated. The type of reaction can also be notable as endothermic reactions entail more energy to be supplied to them and so give positive peaks in the trace, and exothermic reactions result in negative peaks. DSC runs were carried out using a Perkin-Elmer DSC6 instrument. The experimental traces were recorded at a heating rate of 10 K min^{-1} and under an inert atmosphere of nitrogen gas with a flow rate of 20 cm^3 min^{-1}. The sample masses ranged between 2-4 mg. This method uses two identical 50 µL crimped and vented aluminium pans, one contains a sample and the other is empty and used as a reference. The DSC was calibrated by measuring the onset temperature of indium (156.6 °C) while the heat flow was calibrated from the enthalpy of fusion of indium (28.62 J g^{-1}).

Thermogravimetry (TG)

In thermogravimetric (TG) analysis, a sample is heated at a constant rate and the loss of mass as a function of temperature is measured as the compound degrades. TG measurements were performed using a Perkin Elmer PC6-Series more specifically PE-TGA6 under dry N_2 gas purge with a flow rate of 20 cm^3 min^{-1} at 10 °C min^{-1}. Measurements were taken from 30 – 300 °C.

KINETICS

Kinetics of desolvation were investigated non-isothermally using TG techniques. [1] The thermogravimetric rate is given by: $dC/dT = (A/B)\ f(C)\ e^{-E/RT}$, where C = degree of mass loss and β = scan rate. This equation can be reduced to: $d\log \beta/dT^{-1} = (0.457/R)\ t$. TG experiments were conducted at various scan rates ranging from 2 – 15 °C min^{-1}. The resultant curves were analysed by plotting $-\log \beta$ vs T^{-1} where T = absolute temperature. An activation energy range could then be computed. The sample was removed from its mother liquor and crushed using filter paper to form a powder. Solid-solid reaction kinetics was also performed using powder x-ray diffraction (PXRD) which is described in the PXRD section below. Two solids (host and the guest) were ground together using an agate mortar and pestle at room temperature. The starting quantities of the reactants were in the same stoichiometries as given by the crystal structure analyses. Samples were withdrawn at different times and analysed by PXRD. The kinetics of the solid – solid reactions were monitored by selecting the appearance or disappearance of a particular peak in the newly forming inclusion compound. Diamond powder was added to the samples and the peak of diamond was used as a calibrant.

POWDER X-RAY DIFFRACTION (PXRD)

PXRD is used to observe the phase changes as well as reaction kinetics for certain inclusion compounds. It is a basic tool for the identification of compounds as each compound shows a unique pattern due to its particular structural features. Manually ground powdered samples were placed on X-ray insensitive Mylar film. The intensities were measured using a Hüber Imaging Plate Guinier Camera 670 using nickel-filtered CuKα_1 (1.54059 Å) radiation produced at 40 kV and 20 mA by a Philips PW1120/00 generator fitted with a Hüber long fine-focus tube PW2273/20 and a Hüber Guinier Monochromator Series 611/15. All PXRD experiments were completed at the University of Cape Town. LAZY PULVERIX [2] was used to generate the idealized X-ray powder traces for known inclusion compounds. Comparisons were then made to identify the compound under investigation.

DATA COLLECTION

Crystal structure analysis

Crystals of good quality and suitable size were selected for X-ray photography and data collections. They were immersed in Paratone N oil and mounted on a glass fibre for data collection at low temperatures (133 K) using the Nonius Kappa-CCD diffractometer, using 1.2 kW monochromated MoKα radiation (λ=0.7107 Å) generated by a Nonius FR590 generator produced at 54 kV and 23 mA. For all the structures, the intensity data were collected by the standard phi scan and omega scan techniques and scaled and reduced using the program Denzo – SMN [3]. The program X-Seed [4] was used as a graphical interface. The tactics for data collections were evaluated using COLLECT [5] software.

All the structures were solved by direct methods using SHELXS-86. [6] This process was facilitated by the program XPREP.[7] The structure refinement was done by using the program SHELXL-97[8], which uses full-matrix least-squares minimization of the function ($\Sigma w(F_o^2\text{-}kF_c^2)^2$). The agreement between the observed (F_o) and the calculated (F_c) structure factors is expressed by the residual index, R, which is an indirect measure of the accuracy of the structure and should be low if the model is satisfactory. The residual index, R_1, is the agreement between the observed and calculated structure factors based on F (see equation 1), while the residual index, wR_2, is the agreement based on F^2 (see equation 2).

$$R_1 = \frac{\Sigma\left\|F_0\right| - \left|F_C\right\|}{\Sigma\left|F_0\right|} \qquad (1)$$

$$wR = \sqrt{\frac{\Sigma w\left(F_0^2 - F_C^2\right)^2}{\Sigma w\left(F_0^2\right)}} \qquad (2)$$

w is the weighting scheme and was refined for each structure:

$$w = \frac{1}{\sigma^2 F_0^2 + (aP)^2 + bP} \qquad (3)$$

$$\text{where } P = \frac{\max\left(0, F_0^2\right) + 2F_c^2}{3} \qquad (4)$$

Both a and b were refined for each structure.

The Goodnesss of Fit (S) was also determined for each structure and is based on F^2 (equation 5)

$$S = \left(\frac{\Sigma w\left(F_0^2 - F_c^2\right)^2}{n - p}\right)^{\frac{1}{2}} \qquad (5)$$

where n is the number of reflections and p is the total number of parameters refined.

Additional Computing Packages

A number of computing packages included in the graphical interface software X-seed[4] were used in this study:

- Layer[9]
  - Intensity data is displayed as simulated precession photographs of the reciprocal lattice levels and allows for the investigation of the systematic absences which occur.
- Lazy Pulverix[2]
  - Calculates the theoretical X-ray powder diffraction pattern from single crystal data.
- Section[10]
  - Gives a graphical interpretation of the packing in the structure, by effectively cutting slices through the unit cell. The guest molecules can be removed and the host shown with its van der Waals radii so that channels or cavities can be investigated.
- PovRay[11]
  - Renders graphics for structures.

Other programs used that were not included in X-seed[4]:

- Xprep[7]
  - Sets up SHELX input files and determines the space group, also allows the input of space group not determined as well as unit cell transformations.
- Platon[12]
  - Calculates all molecular parameters for the structures.

- ConQuest[13]
  - Search engine using the Cambridge Structural Database (CSD) for informative and comparative structure details.

REFERENCES

1. Flynn, J. H.; Wall, L. A.; J. *Polym. Sci; Part B: Polym. Lett*. **1966,** 4,323.
2. Yvon, K.; Jeitschko, W.; Parthé, E. *J. Appl. Crystallogr*. **1977,** 10, 73-74.
3. Otwinowski, Z.; Minor, W.; Methods in Enzymology; Macromolecular Crystallography; Part A; Carter, C. W. and Sweet, R. M.; Eds.; Academic Press; New York; **1997,** 276, 307 – 326.
4. Barbour, L. J.; X-Seed; Graphical Interface for the SHELX program; *J. Supramol. Chem*. **2003,** 1, 189,
5. COLLECT; Data Collection Software; Nonius; Delft; The Netherlands; **1999**.
6. Sheldrick, G. M.; SHELXS-86; *Crystallographic Computing 3*. eds Sheldrick, G. M.; Kruger, C.; and Goddard, R.; *Oxford Univ. Press*; **1985**.
7. XPREP; Data Preparation & Reciprocal Space Group Exploration; Version 5.1/NT; © **1997**; Bruker Analytical X-ray Systems.
8. Sheldrick, G. M.; SHELXL-97; Program for Crystal Structure Determination; University of Göttingen; Germany; **1997**.
9. Barbour, L. J.; LAYER; A computer program for the graphic display of intensity data as simulated precession photographs; *J. Appl. Cryst*. **1999,** 32, 351.
10. Barbour, L. J.; LAYER; A computer program for the graphic display of cross sections through a unit cell; *J. Appl. Cryst*. **1999,** 32, 353.
11. Pov-Ray for Windows; Version 3.1e.watcom.win32; The persistence of Vision Development Team; © **1991-1999.**
12. Spek, A. L.; PLATON; A multipurpose crystallographic tool; Version 10500; © **1980-2000.**
13. ConQuest; A program for the search of the CSD; Version 1.7; © CCDC **2001.**

CHAPTER 3

RESULTS AND DISCUSSION

PART ONE

RESULTS AND DISCUSSION

The inclusion compounds formed between the host 9-(4-methoxyphenyl)-9H-xanthen-9-ol (A1) and the guests 1-naphthylamine (**NAPH**), 8-hydroxyquinoline (**HQ**), 1,4-diazabicyclo[2.2.2]octane (**DABCO**), acridine (**ACRI**) and benzaldehyde (**BENZAL**) will be discussed. The thermal stabilities, kinetics of desolvation, solid – solid kinetics and crystal structure were studied. Labelling of the host, A1, is given below with the guests included.

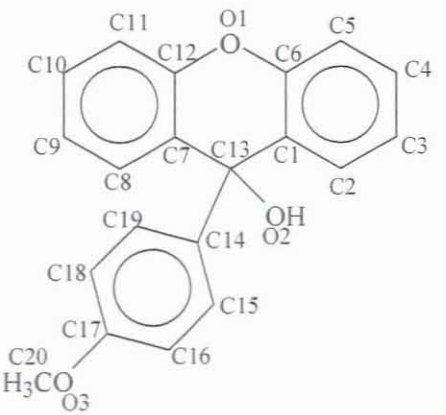

9-(4-methoxyphenyl)-9H-xanthen-9-ol

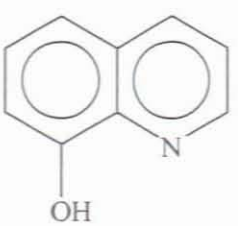

8-hydroxyquinoline

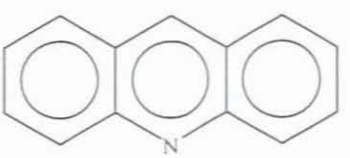

Acridine

1,4-diazabicyclo[2.2.2]octane

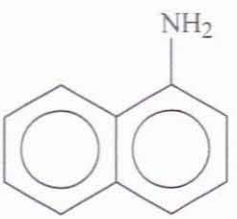

1-naphthylamine

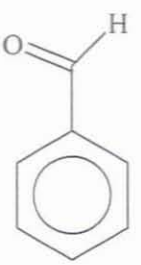

Benzaldehyde

Scheme 4 Host 9-(4-methoxyphenyl)-9H-xanthen-9-ol and guests

Thermal analysis

Thermogravimetry was not performed on the four inclusion compounds (**A1·ACRI**, **A1·½DABCO**, **A1·½NAPH** and **A1·½HQ**). The host:guest ratios were determined using nuclear magnetic resonance spectroscopy. Thermal profiles of the single crystals, grown from solution, of each inclusion compound by differential scanning calorimetry were analysed. For each compound a single endotherm corresponding to its melting point was obtained. The results are summarised in Table 4.

Inclusion Compound	**A1·ACRI**	**A1· ½ DABCO**	**A1· ½ NAPH**	**A1·½HQ**
H:G ratios	1:1	1: ½	1: ½	1: ½
DSC (T_{on}/K) Endotherm C	426.9	443.0	413.4	399.2
Melting Point of guest (K) Endotherm A	380.7	429.7	322.2	346.5
Melting Point of host (K) Endotherm B	395.2			

Table 4 Summary of the DSC results

The following DSC curves show the results obtained for the guest alone (endotherm A in red), the host alone (endotherm B in blue) and the inclusion compound (endotherm C in purple).

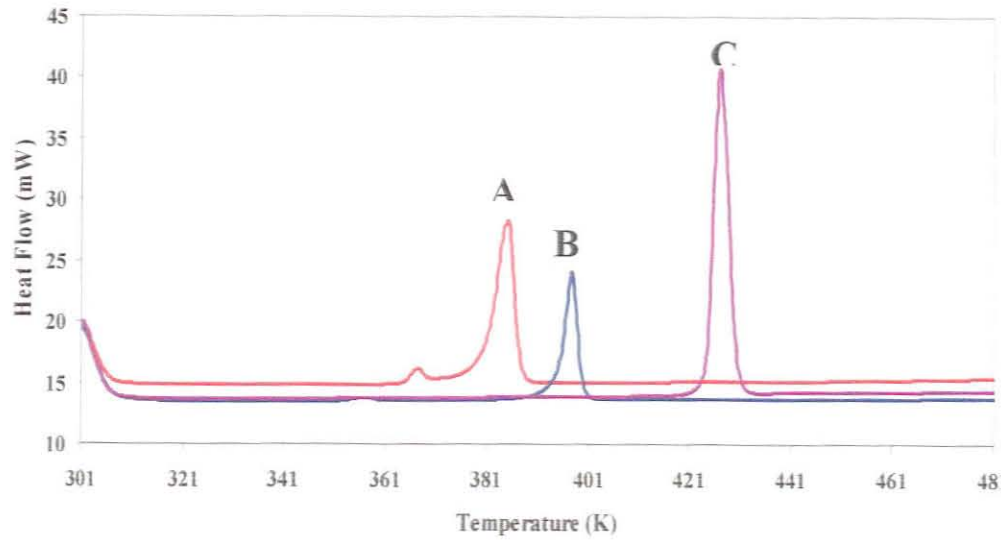

Figure 6 A = melt of **ACRI**; B = melt of **A1**; C = melt of **A1·ACRI**.

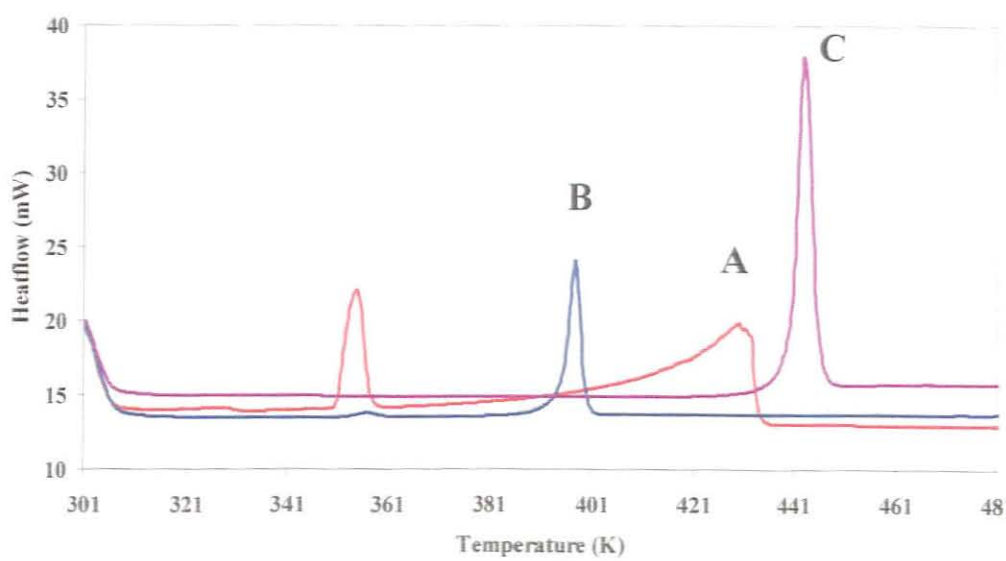

Figure 7 A = first peak is due to a phase change, second peak is due to a melt of **DABCO**; B = melt of **A1**; C = melt of **A1·½DABCO.**

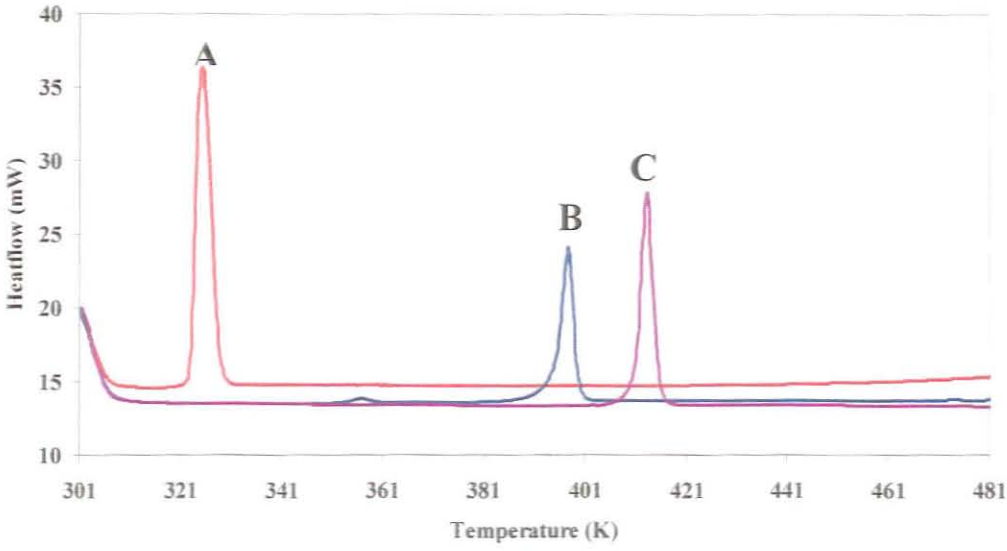

Figure 8 A = melt of **NAPH**; B = melt of **A1**; C = melt of **A1·½NAPH**.

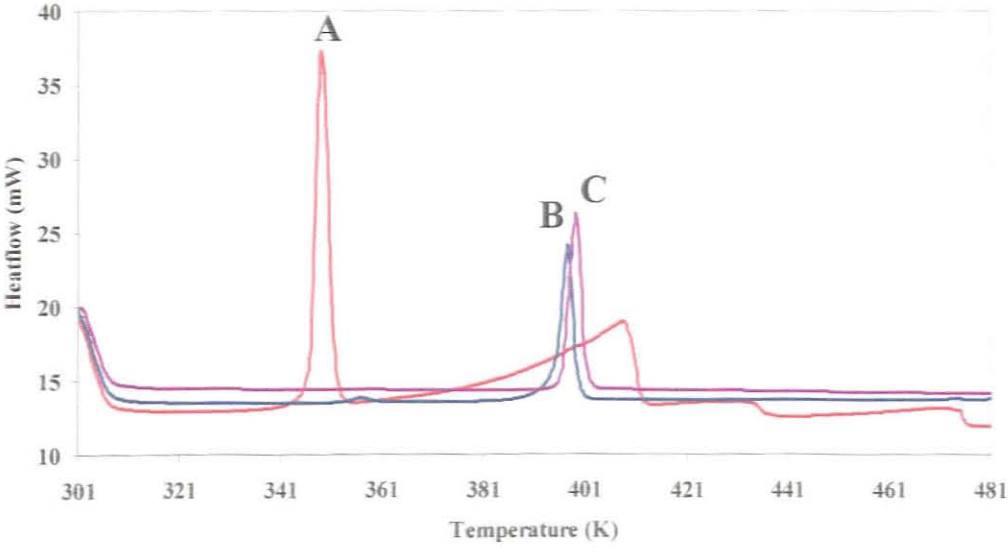

Figure 9 A = melt of **HQ**, second broad peak is due to a phase change; B = melt of A1; C = melt of **A1·½HQ**.

Discussion

The melting point of the inclusion compounds was found to be higher than that of the host or the respective guest. The **DABCO** compound shows high stability with the melting point 48 K higher than that of the apohost. This could be attributed to the two hydrogen bonds that link the **DABCO** guest to the host A1. For the 1-naphthylamine and the 8-hydroxyquinoline structures there are no hydrogen bonds between the host and the guests. For the **A1·ACRI** structure a single hydrogen bond links the host molecules to the acridine guest. These interactions are discussed in greater detail later in this chapter.

For the liquid guest benzaldehyde both TG and DSC were performed. The TG curve shows a single step which is due to the loss of the guest. The DSC shows two endotherms, the first endotherm can be attributed to the loss of the benzaldehyde guest and the second endotherm can be attributed to the host melt which is broad and not well defined (Fig 10).

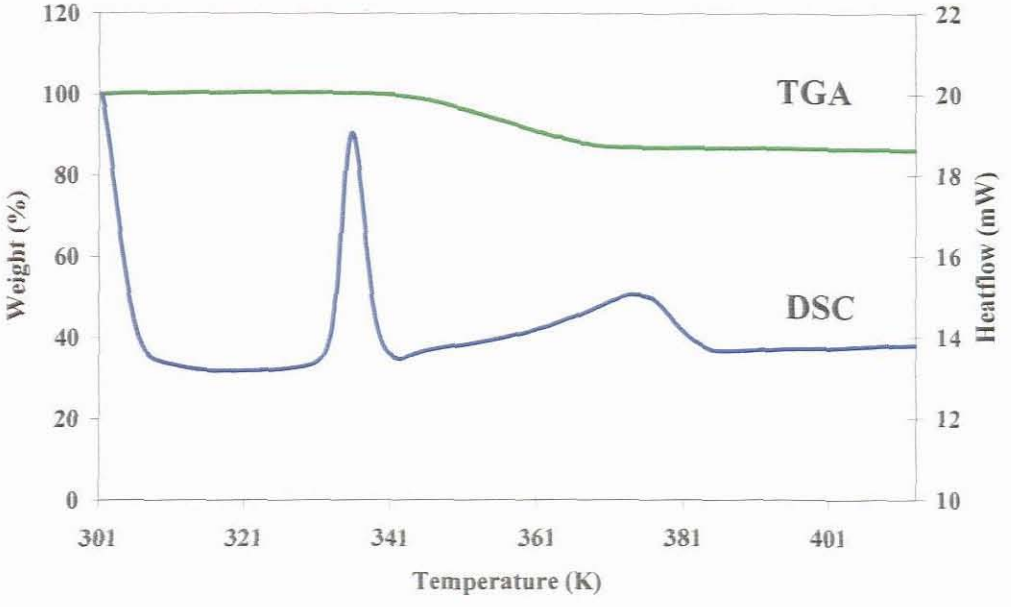

Figure 10 Thermal analysis curves for **A1·½BENZAL**.

Kinetics of desolvation

Kinetics of desolvation for **A1·½BENZAL** were carried out using the method of Flynn and Wall [1] in which the mass loss was recorded as a function of temperature at selected heating rates (β) varying from 2 K min^{-1} to 15 K min^{-1} (Fig 11). The plots of $-\log \beta$ versus T^{-1} are shown in Fig 12. The graph is plotted for different extents of decomposition varying systematically from 2% to 10%. The lines are practically parallel indicating an unchanging mechanism of desorption, corresponding to an activation energy of 74 kJ mol^{-1} – 86 kJ mol^{-1}.

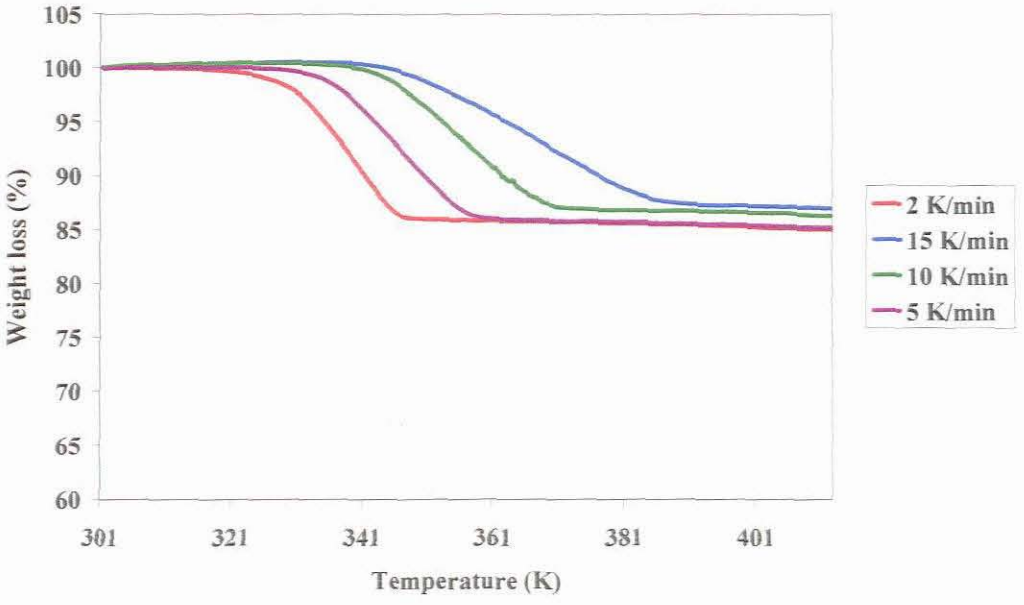

Figure 11 TG curves of **A1·½BENZAL** for the different heating rates.

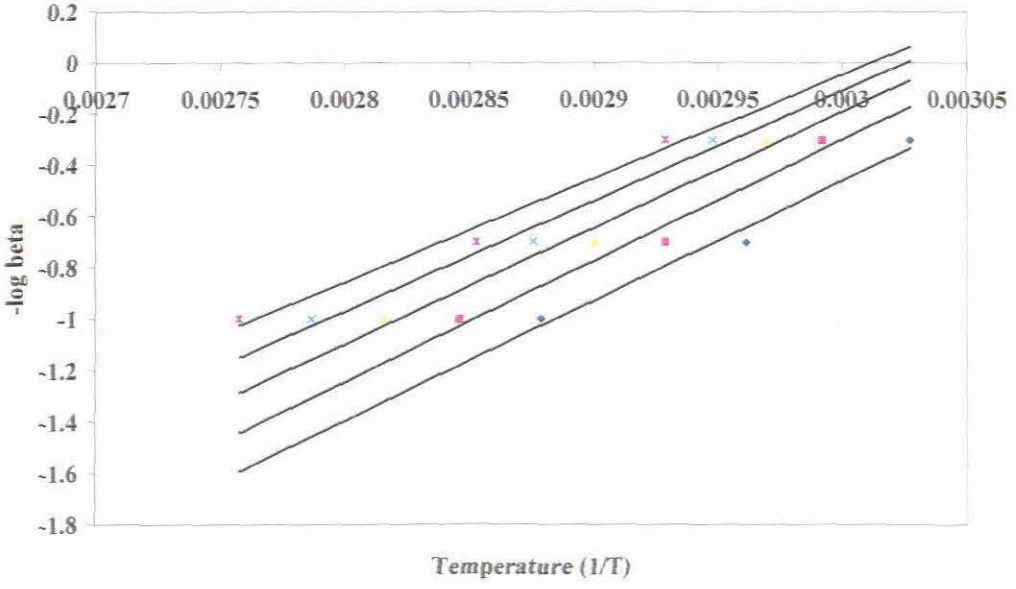

Figure 12 Plot of - log β versus T^{-1} for **A1·½BENZAL**

Discussion

The activation energy of benzaldehyde with host **A1** compares favourably with the value of 80 – 90 kJ mol^{-1} obtained for the compound 9-(4-methylphenyl)-9H-xanthen-9-ol with cyclohexanone.[2] For the dioxane compound with this host A1 [3] the guest lies in highly constricted channels and the activation energy was in the range 133 – 162 kJ mol^{-1}.

Kinetics of solid – solid reactions

The grinding experiments were carried out with an agate mortar and pestle at room temperature. The starting quantities of the reactants were in the same stoichiometries as given by the crystal structure analyses. Samples were withdrawn at fixed periods of time and the ground powders analysed by PXRD. The results for each compound are shown in the figures below. The kinetics of the solid – solid reactions were monitored between the apohost and the various guests by selecting the appearance of a particular peak in the newly forming inclusion compound. The grinding experiment was interrupted at chosen intervals and fixed quantities of diamond powder were added to the samples. The intensities of the targeted peak were measured using the diamond peak as a calibrant.

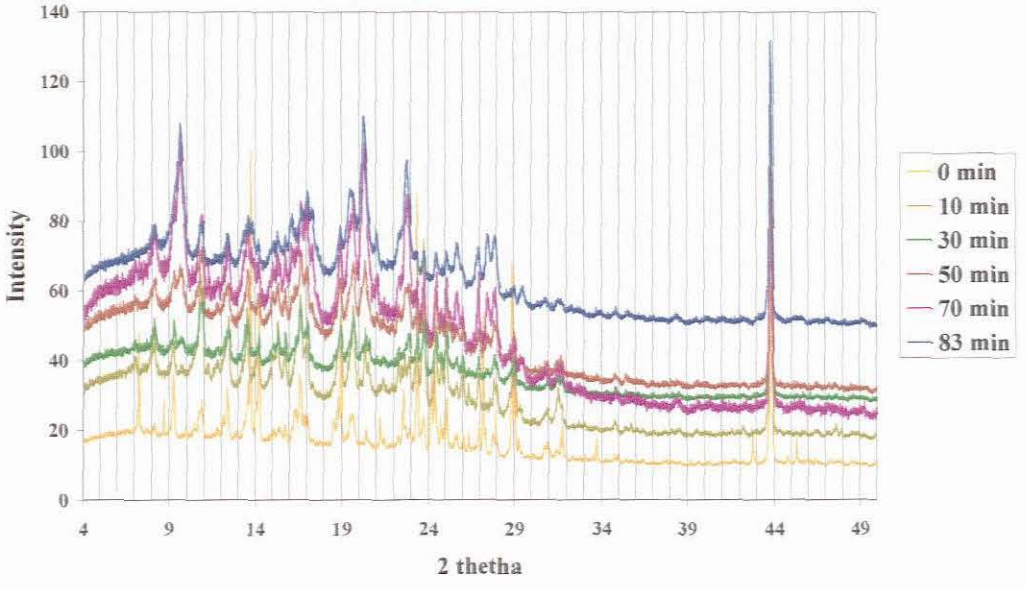

Figure 13 PXRD traces of **A1·ACRI** after different time intervals. The peak at 2θ = 8° was used for the kinetics.

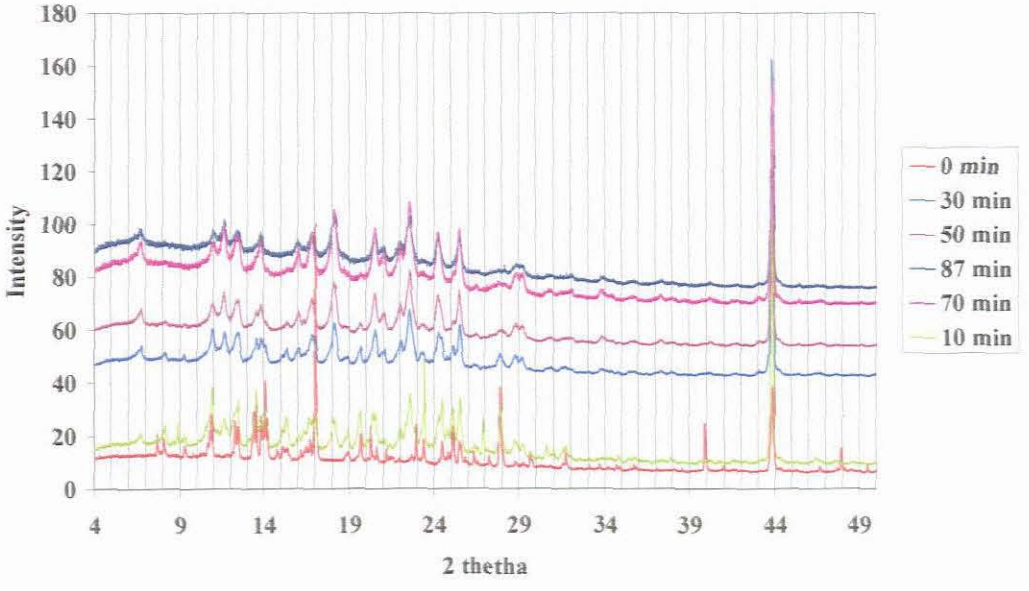

Figure 14 PXRD traces of **A1·½HQ**. The peak at 2θ = 6.8° was used for the kinetics.

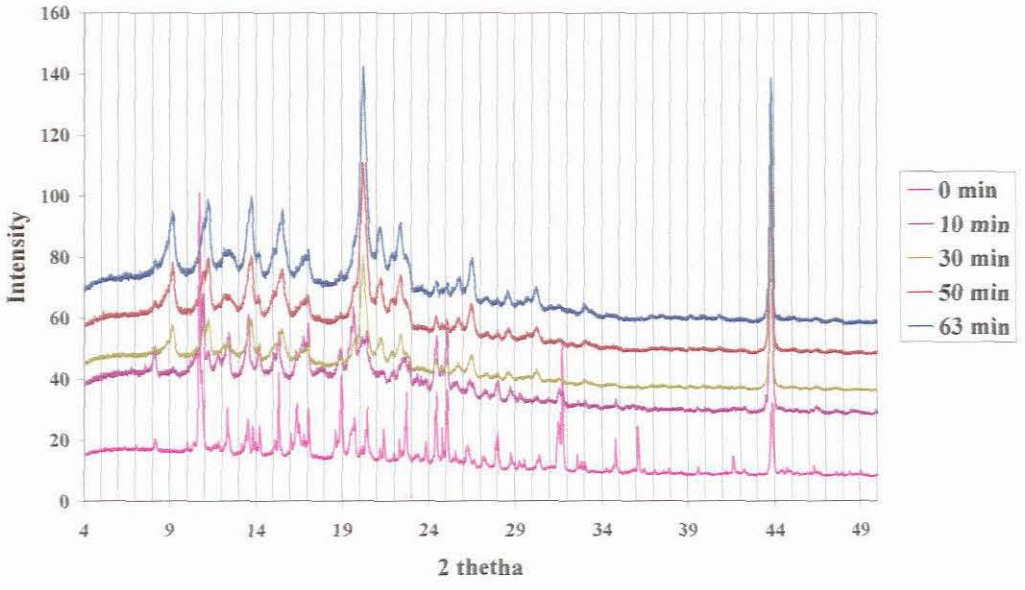

Figure 15 PXRD traces of **A1·½DABCO**. The peak at 2θ = 9.1° was used for the kinetics.

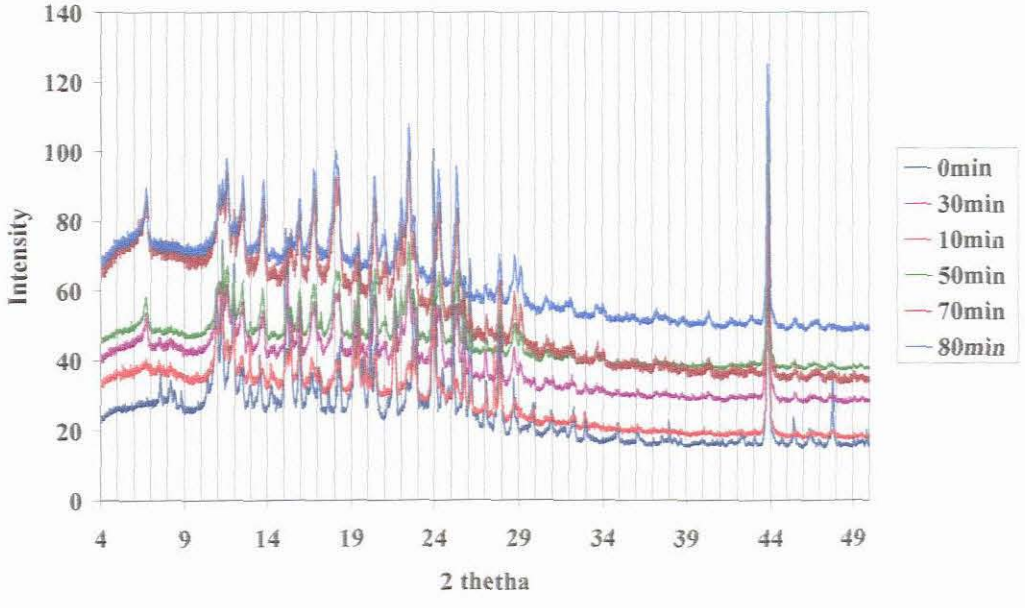

Figure 16 PXRD traces of **A1·½NAPH**. The peak at 2θ = 6.8° was used for the kinetics.

Discussion

The results of the solid – solid reactions are shown in Fig 17 in which ln (1-α) vs time was plotted for each compound, where α represents the extent of reaction as measured by the normalised intensity of a targeted diffraction peak of the product. The solid-solid reactions therefore follow first order kinetics: $\ln(1-\alpha) = -kt$. The rate constants for the solid – solid reactions, carried out at ambient temperature (298 K) were calculated as follows:

- **A1· ½ NAPH** $k = 1.85 \times 10^{-2}\ min^{-1}$
- **A1·½HQ** $k = 2.20 \times 10^{-2}\ min^{-1}$
- **A1·½DABCO** $k = 2.51 \times 10^{-2}\ min^{-1}$
- **A1·ACRI** $k = 6.10 \times 10^{-3}\ min^{-1}$

The kinetics for the **A1·ACRI** reaction is significantly slower than those of the other three compounds. This could be attributed to the estimated lower vapour pressure of acridine [4] at 298 K compared to the other three guests.

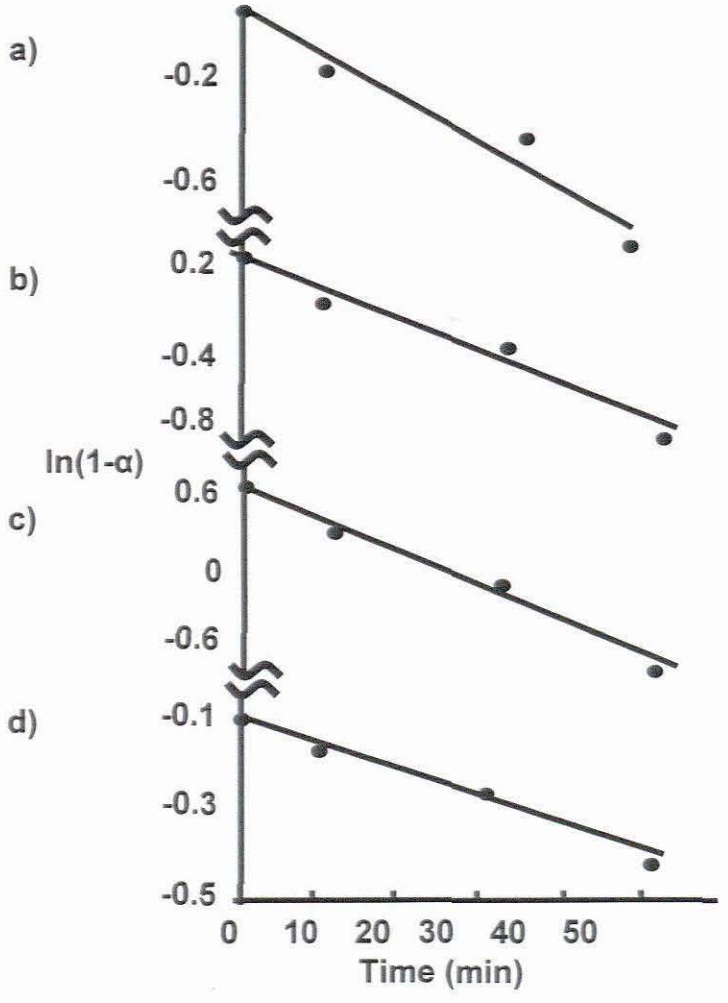

Figure 17: First order kinetics plots for a) **A1·½NAPH**, b) **A1·½HQ**, c) **A1·½DABCO** and d) **A1·ACRI**

Solid-solid grinding experiments were conducted to determine whether the inclusion compounds could be synthesised without the use of solvent. The compounds obtained from the grinding experiments were compared to the calculated powder patterns obtained from the single crystal structure using LAZY PULVERIX.[5] They are all shown in the figures below:

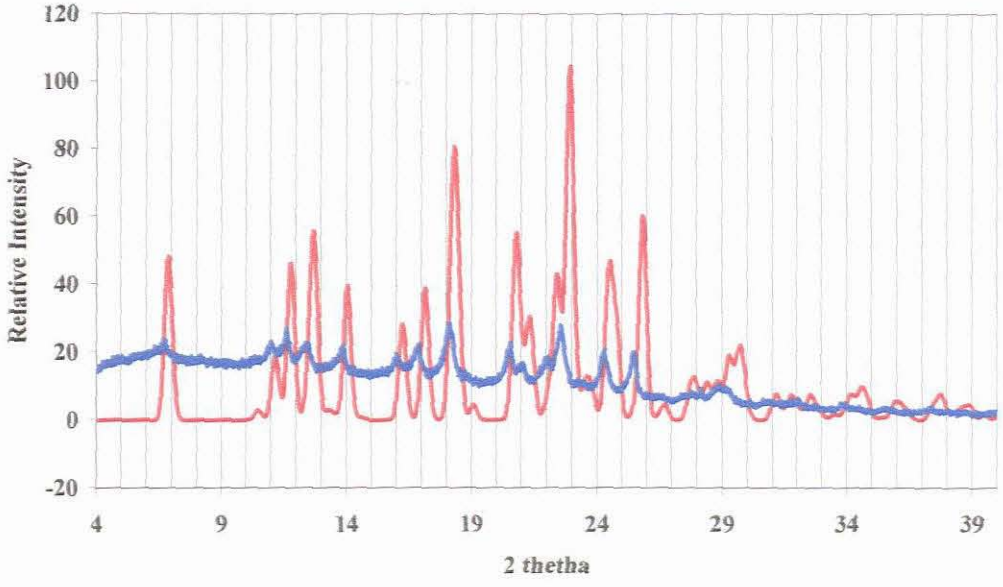

Figure 18 Comparison between the experimental (blue) and the calculated (red) powder pattern of **A1·½HQ**.

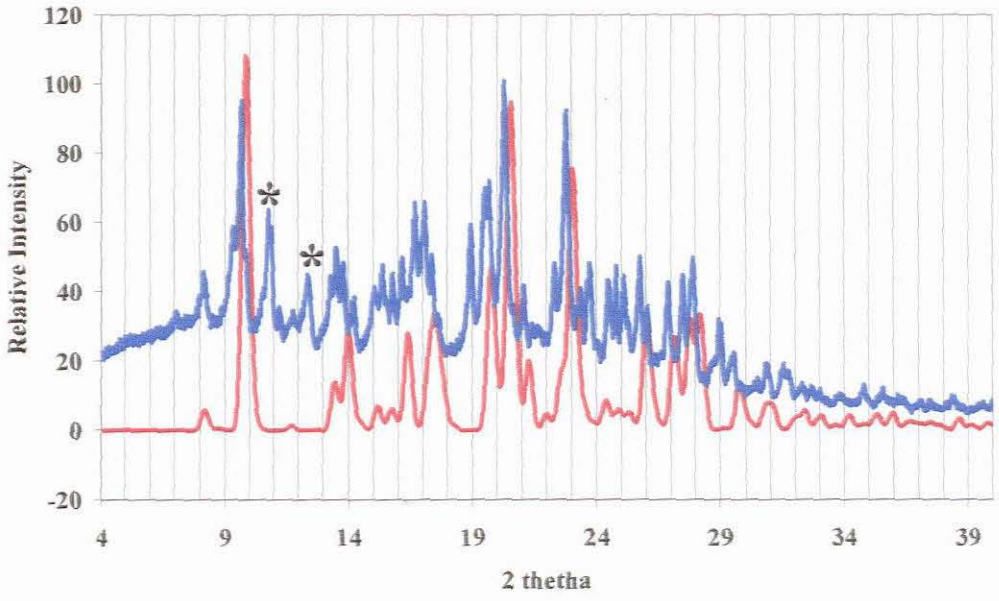

Figure 19 Comparison between the experimental (blue) and the calculated (red) powder pattern of **A1·ACRI**. Peaks marked * are due to starting material, reaction did not go to completion.

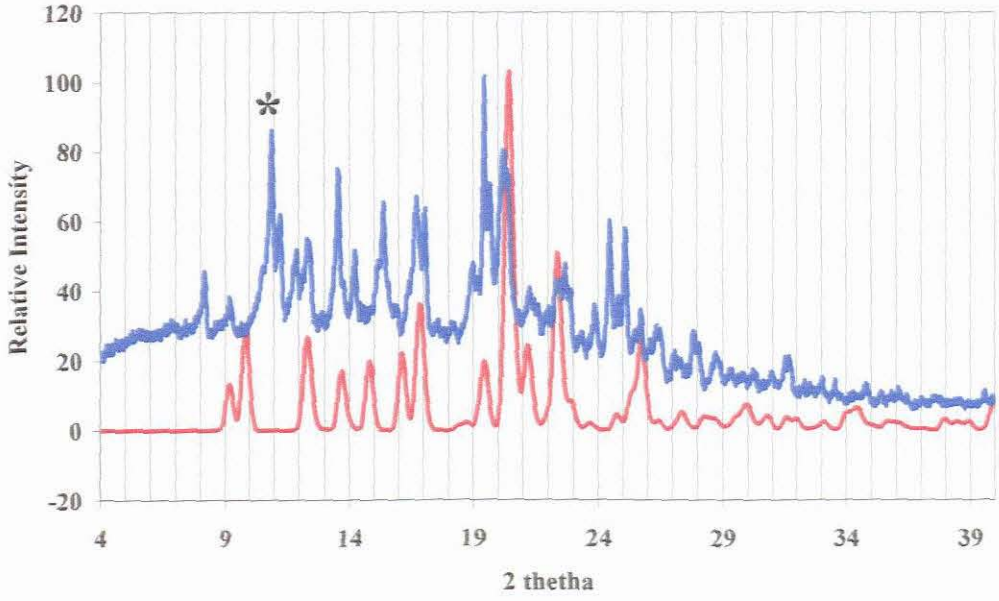

Figure 20 Comparison between the experimental (blue) and the calculated (red) powder pattern of **A1·½DABCO**. Peak marked * is due to starting material, reaction did not go to completion.

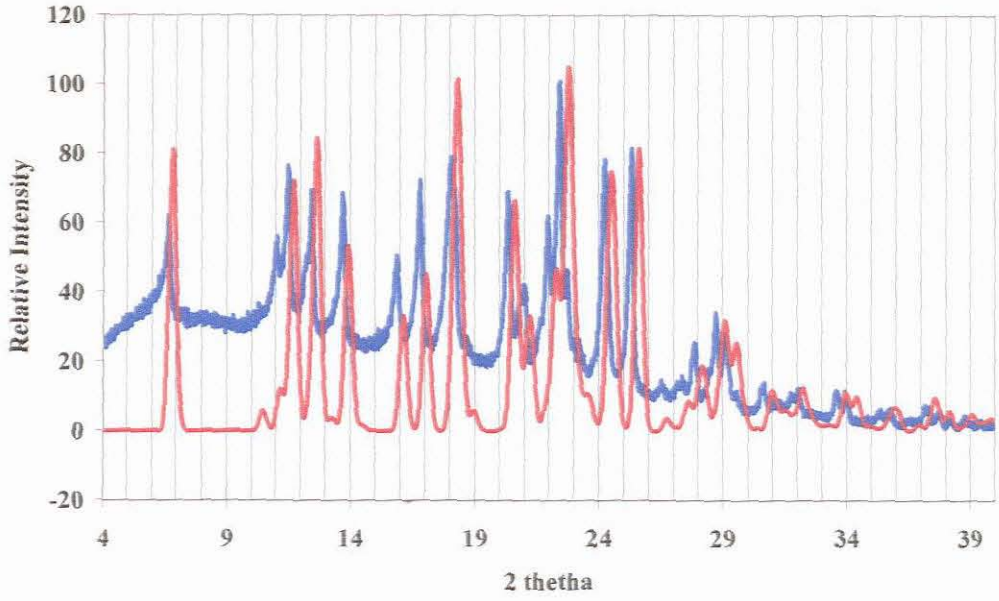

Figure 20 Comparison between the experimental (blue) and the calculated (red) powder pattern of **A1· ½ NAPH**.

In general there is good agreement between the experimental and the calculated powder patterns. For the **A1·ACRI** and the **A1·½DABCO** compounds the reactions did not proceed to completion.

STRUCTURE DETERMINATION

The host and each of the guest compounds 1-naphthylamine, 8-hydroxyquinoline, acridine and 1,4-diazabicyclo[2.2.2]octane were dissolved in ethanol in 1:1 ratios and the saturated solutions were allowed to crystallise at room temperature. Cell dimensions were established from the intensity data measured on a Kappa CCD difractometer using graphite – monochromated Mo-K_α radiation. The strategy for the data collections was evaluated using COLLECT [6] software. The structures were solved by direct methods and refined by full matrix least – squares with SHELX-97 [7] refining on F^2.

	A1·½NAPH	**A1·½HQ**	**A1·½DABCO**	**A1·ACRI**	**A1·½BENZAL**
Compound	A1[a]·½$C_{10}H_9N$	A1[a]·½C_9H_7NO	A1[a]·½$C_6H_{12}N_2$	A1[a]·$C_{13}H_9N$	A1[a]·½C_7H_6O
M/g mol^{-1}	375.42	376.90	360.42	483.54	357.41
T/K	173 K	173 K	173 K	173 K	173 K
Crystal System	triclinic	triclinic	triclinic	triclinic	monoclinic
Space group	$P\ \bar{1}$	$P\ \bar{1}$	$P\ \bar{1}$	$P\ \bar{1}$	$P2_1/n$
a/Å	8.4231(17)	8.3982(17)	9.057(18)	10.607(2)	12.869(3)
b/Å	9.0634(18)	8.9905(18)	9.6751(19)	11.247(2)	9.5808(19)
c/Å	13.014(3)	12.954(3)	10.501(2)	11.967(2)	15.929(3)
α/°	96.60(3)	96.36(3)	88.56(3)	96.17(3)	90
β/°	91.87(3)	91.64(3)	83.74(3)	110.43(3)	113.80(3)
γ/°	109.87(3)	109.193)	85.45(3)	111.08(3)	90
V/Å^3	925.4(3)	916.1(3)	911.7(3)	1203.2(4)	1797.0(6)
Z	2	2	2	2	4
μ/mm^{-1}	0.088	0.092	0.086	0.085	0.088
F(000)	395	395	382	508	740
Reflections collected/unique	15208/3505	13605/3435	15587/3431	20116/4553	15937/3348
ρ_{calc}/g cm^{-3}	1.347	1.366	1.313	1.335	1.310
Final R indices [$I > 2\sigma(I)$]	$R_1 = 0.1109$, $wR_2 = 0.3526$	$R_1 = 0.0551$, $wR_2 = 0.1349$	$R_1 = 0.0379$, $wR_2 = 0.0914$	$R_1 = 0.0420$, $wR_2 = 0.0964$	$R_1 = 0.0461$, $wR_2 = 0.1323$
R indices (all data)	$R_1 = 0.1471$, $wR_2 = 0.3939$	$R_1 = 0.0796$, $wR_2 = 0.1544$	$R_1 = 0.0538$, $wR_2 = 0.1003$	$R_1 = 0.0660$, $wR_2 = 0.1108$	$R_1 = 0.0638$, $wR_2 = 0.1542$
Lagest difference peak and hole /e Å^{-3}	1.466 and -0.730	0.971 and -0.465	0.192 and -0.210	0.168 and -0.222	0.348 and -0.353

[a]$C_{20}H_{16}O_3$

Table 5 Crystal data table

A1· ½ NAPH

The structure was solved in the triclinic space group $P\ \bar{1}$. The host molecule was found in a general position with the guest molecule (**NAPH**) located at a centre of symmetry at Wyckoff position *g*, thus Z = 2. The guest was disordered and bond length constraints were imposed such that:

- C1G – C2G = 1.4 Å
- C2G – C3G = 1.4 Å
- C3G – C4G = 1.4 Å
- C4G – C5G = 1.4 Å
- N1G – C3G = 1.4 Å
- N1G – C1G = 2.8 Å
- C2G – C5G = 2.8 Å
- $C2G^{*}$ – C4G = 2.8 Å

where * = -x, -y-1, 1-z.

The guest atoms were restrained to be co – planar.

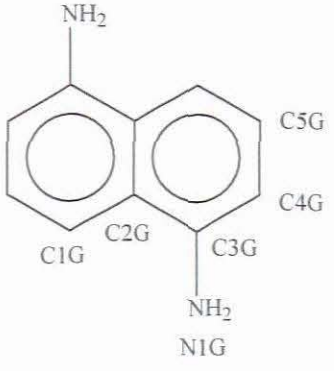

Schematic diagram of 1-naphthylamine (**NAPH**) guests.

The host non – hydrogen atoms were refined anisotropically. Hydrogens were fixed in position such that for aromatic hydrogens the C – H distance = 0.950 Å and for the

methyl hydrogens the C–H distance = 0.980 Å. The guest atoms were refined isotropically. After refinement a residual electron density of 1.47 e $Å^{-3}$ could not be accounted for. The R factor is relatively high due to the disordered guest. The packing down [100] is shown in Fig 21. The host molecules form a centrosymmetric dimer (Host)–OH·····O–(Host) where the hydroxyl group of one host is hydrogen bonded to the pyranyl oxygen of another host and the guest is situated in a channel. Fig 22 shows the channels down [010] with the guest omitted and the host shown in van der Waals radii. The channel dimensions were determined using the program SECTION.[8] The channels are consistent; the dimensions are estimated to be 5.05 Å x 5.91 Å. A comparison of the packing diagram of **A1·½NAPH** and **A1·½BENZ** [9] is shown in Fig 23. The distance, d, between the neighbouring host molecules is approximately 8.423 Å for the 1-naphthylamine structure and approximately 3.333 Å for the benzene structure. This results in the guest situated in cavities for **A1·½BENZ** and in channels for **A1·½NAPH**. The structure is further stabilised by face–to–face π-π stacking between the aromatic rings of adjacent host molecules. The shortest distance between the two centroids of the aromatic rings of neighbouring host molecules is approximately 4.127 Å.

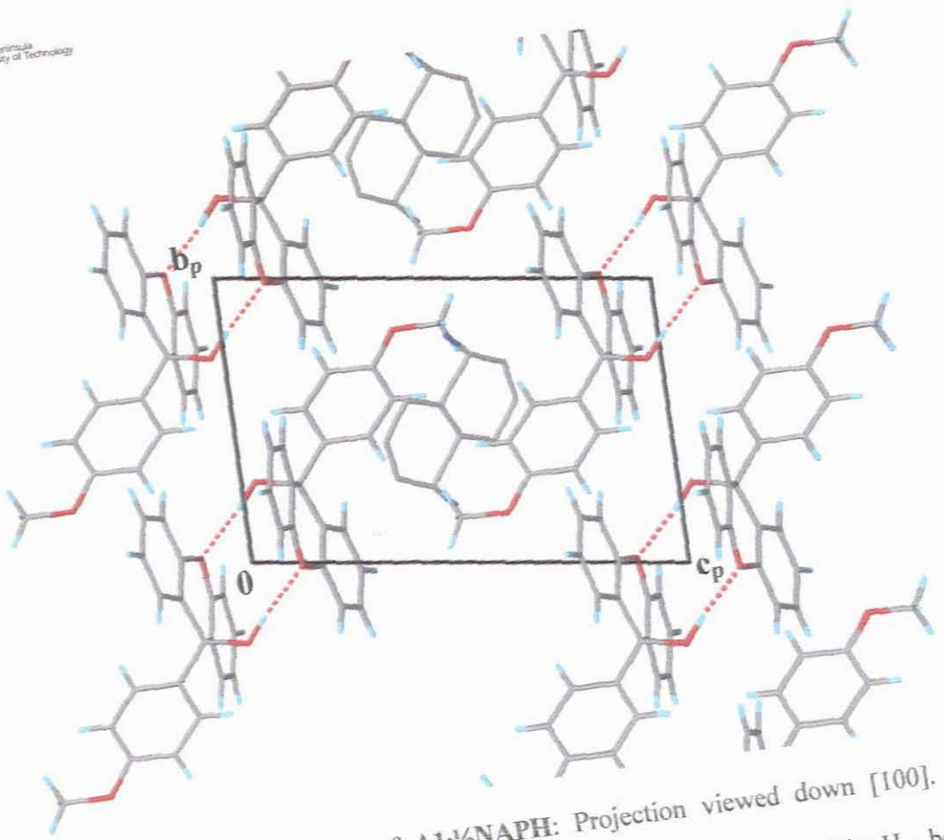

Figure 21 Packing diagram of **A1·½NAPH**: Projection viewed down [100]. All hydrogen atoms except the hydroxyl hydrogen on the host are omitted. The H – bonds are plotted as dotted lines.

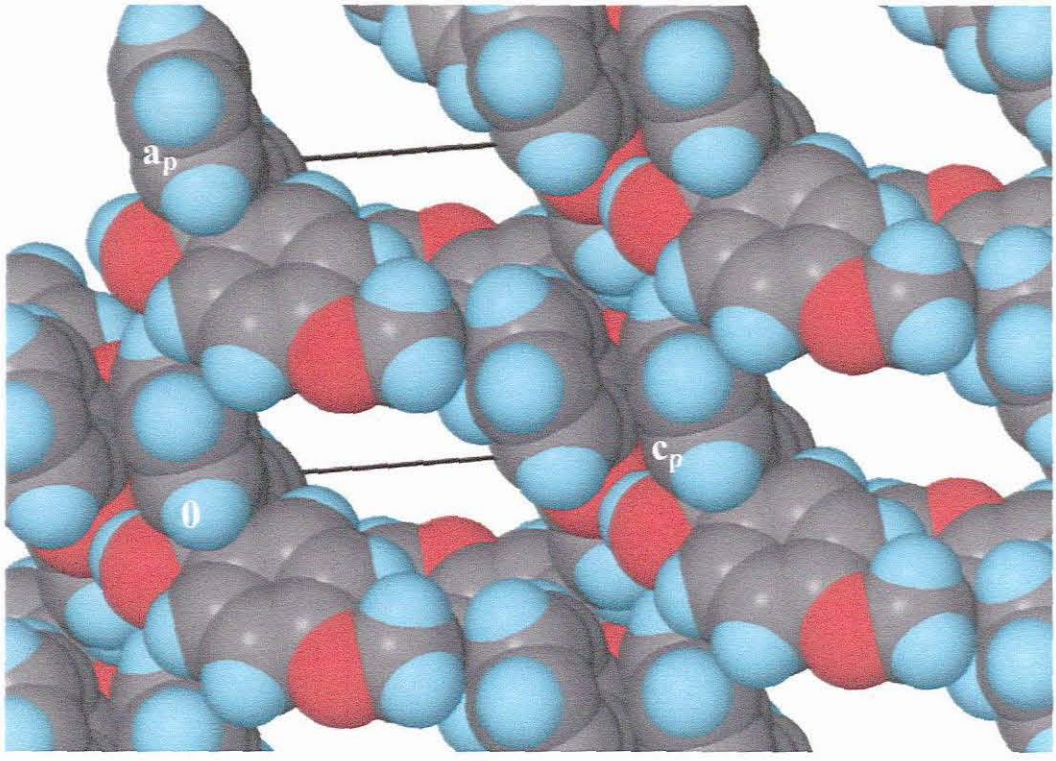

Figure 22 **A1·½NAPH** channels down [010] with the guest omitted and host atoms shown in van der Waals radii.

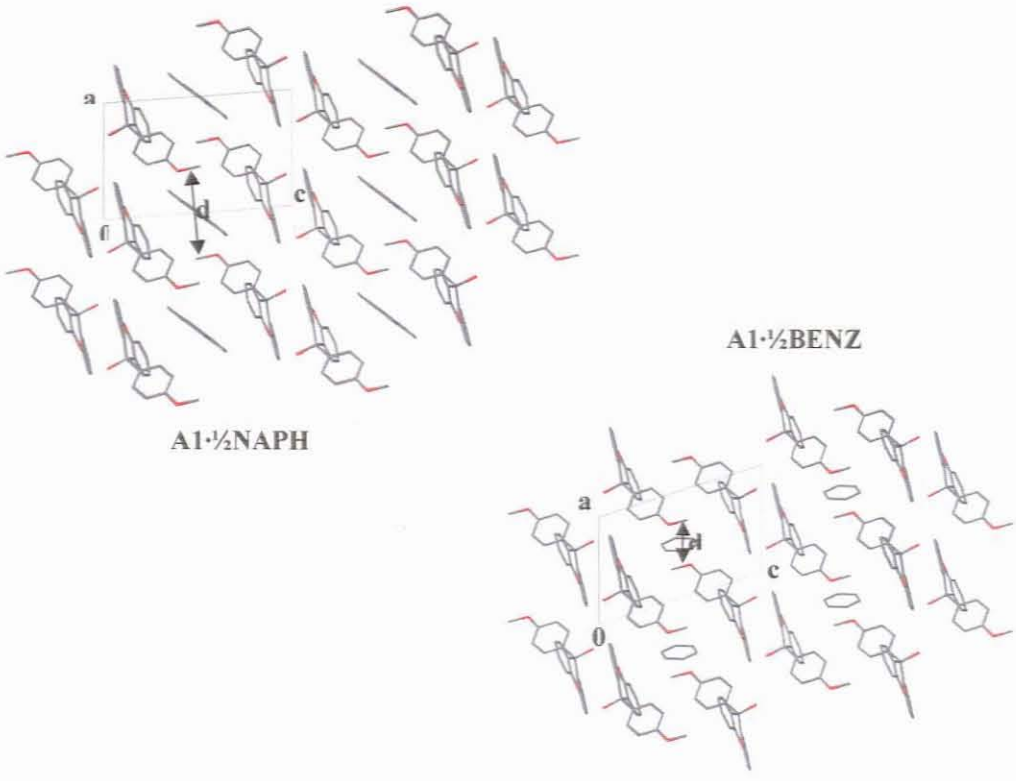

Figure 23 Comparison between **A1·½NAPH** and **A1·½BENZ** viewed down [010].

A1·½HQ

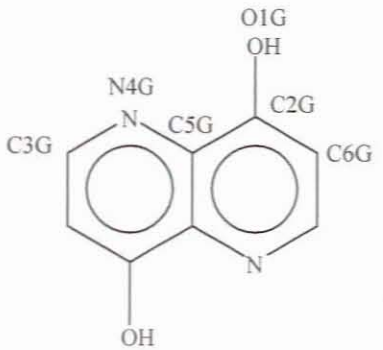

Schematic diagram of 8-hydroxyquinoline (**HQ**) guest.

The structure of **A1·½HQ** is similar to that of **A1·½NAPH**. The structure was solved in the triclinic space group $P\ \bar{1}$. The host was found in a general position with the disordered guest on a centre of inversion at Wyckoff position *c* which is coincident with the midpoint common to the two rings. The hydroxyl moieties and the nitrogen atom are therefore disordered over two positions with equal site occupancies. All hydrogens were treated in the same manner as was observed for the **A1·½NAPH**. Again the host molecules form a centrosymmetric dimer (Host)–OH···O–(Host) and the guest is located in a channel. The channels down [010] are shown in Fig 24 with the guest omitted and the host in van der Waals radii. The channels are consistent; the dimensions are approximately 5.04 Å x 5.89 Å. The packing down [100] with the hydrogen bonding indicated in Fig 25. The packing diagram of **A1·½HQ** with the distance, d, between the neighbouring host molecules approximately 6.013 Å is shown in Fig 26.

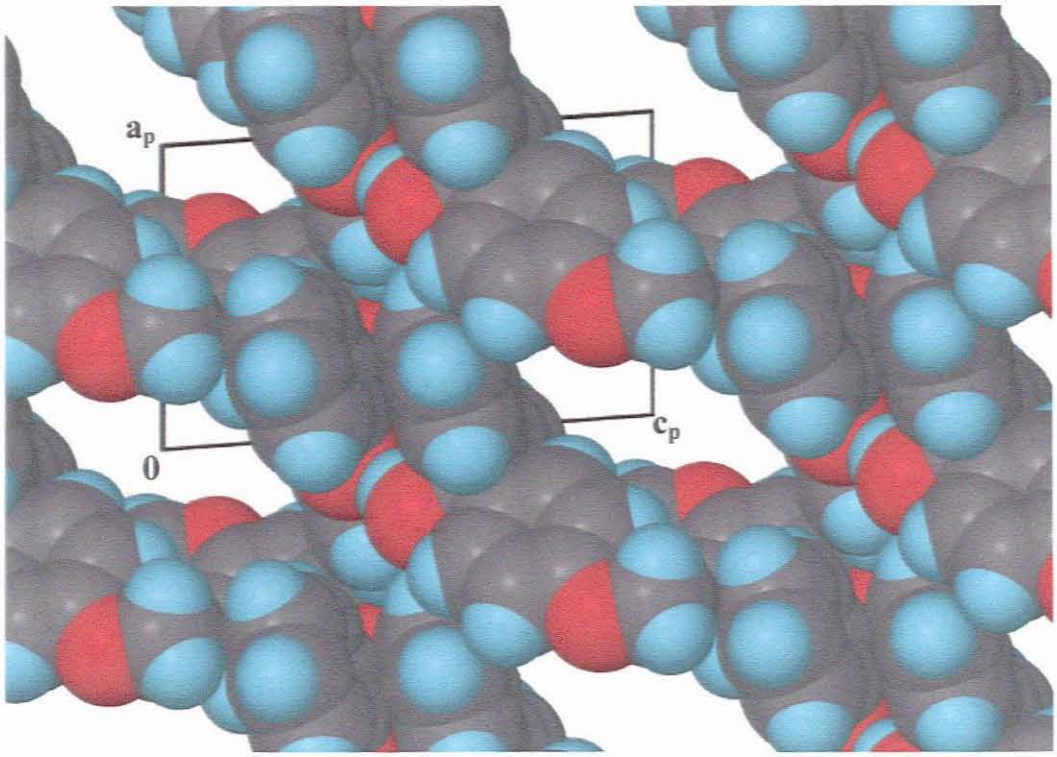

Figure 24 **A1·½HQ** channels down [010].

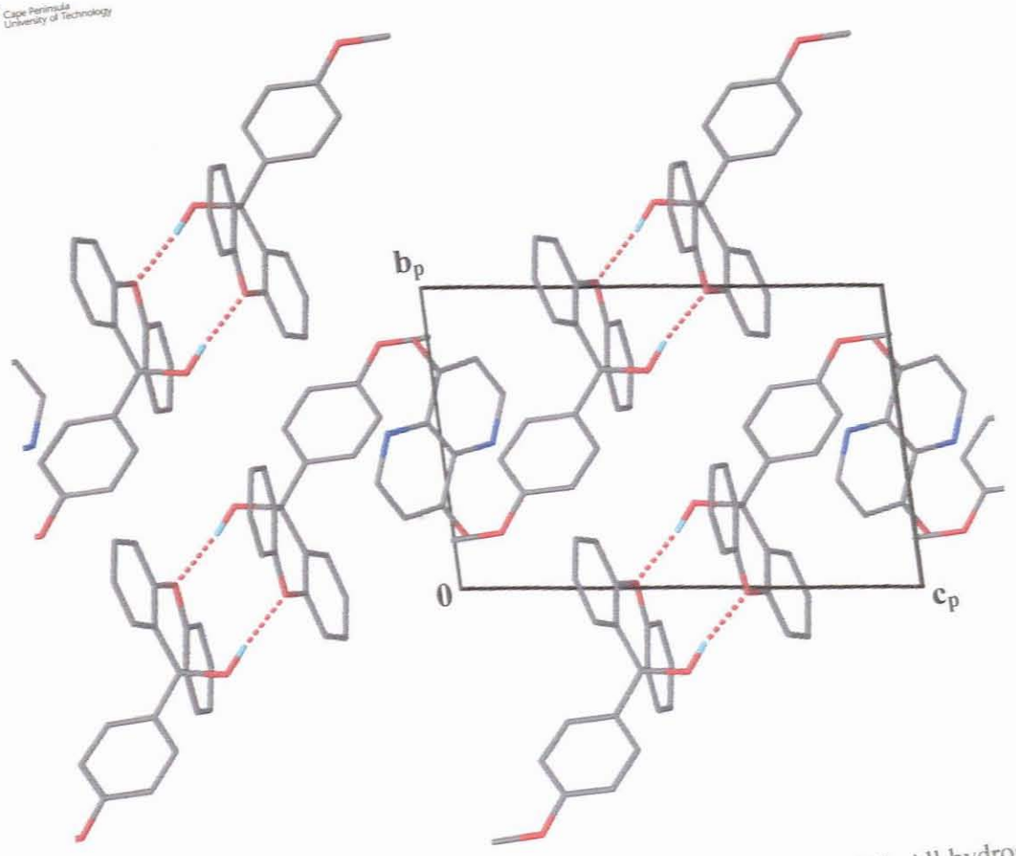

Figure 25 Packing diagram of **A1·½HQ**: Projection viewed down [100]. All hydrogen atoms except the hydroxyl hydrogen on the host are omitted. The H – bonds are plotted as dotted lines.

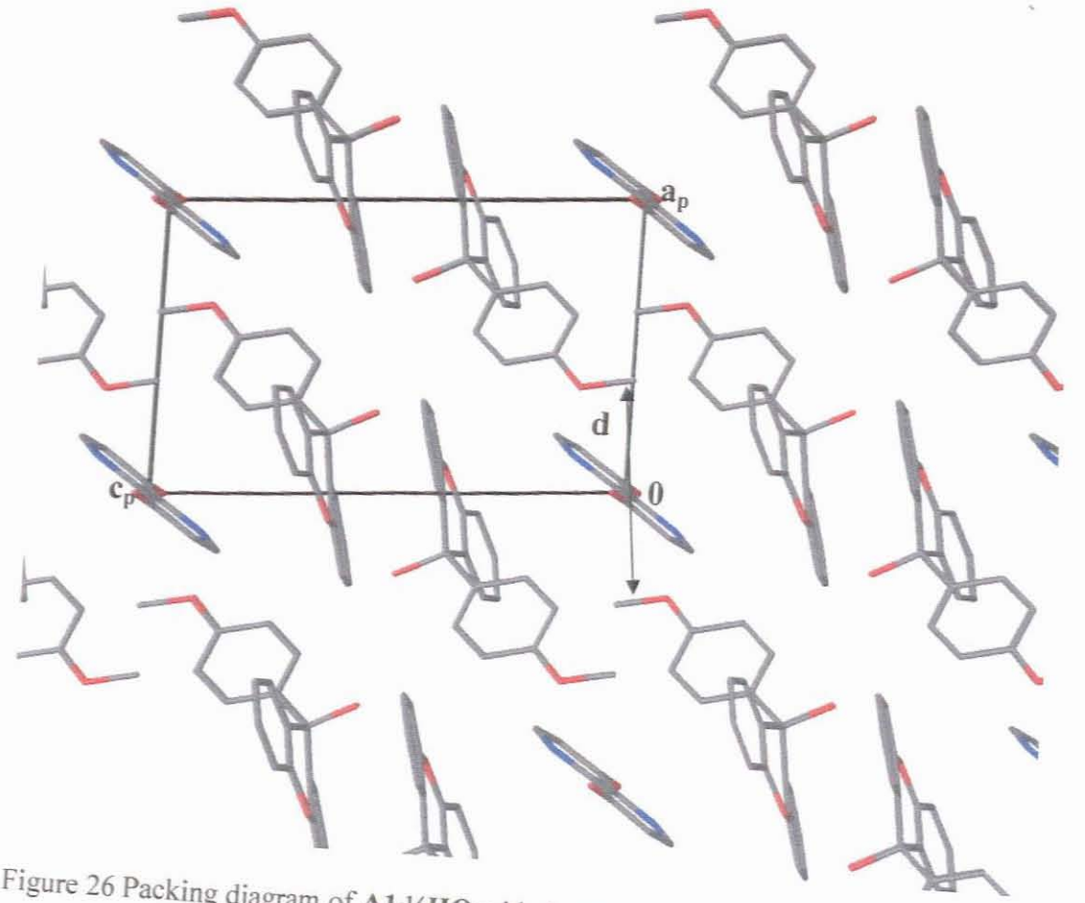

Figure 26 Packing diagram of **A1·½HQ** with d approximately 6.013 Å.

A1·ACRI

The structure was solved in the triclinic space group $P\ \bar{1}$. The structure with the acridine guest has a different stoichiometry to the ones already discussed. The host: guest ratio is 1:1. There is a (Host)–OH···N–(Guest) hydrogen bond as shown in Fig 27. The acridine is not disordered and occupies channels parallel to [100] (Fig 28) and [001] (Fig 29). The dimensions of the channels down [100] are approximately 4.11 Å x 7.26 Å at the wider parts and 4.86 Å x 3.26 Å at the narrower parts, the channels down [001] are estimated to be 6.28 Å x 7.78 Å at the wider parts and 6.63 Å x 3.89 Å at the narrower parts.

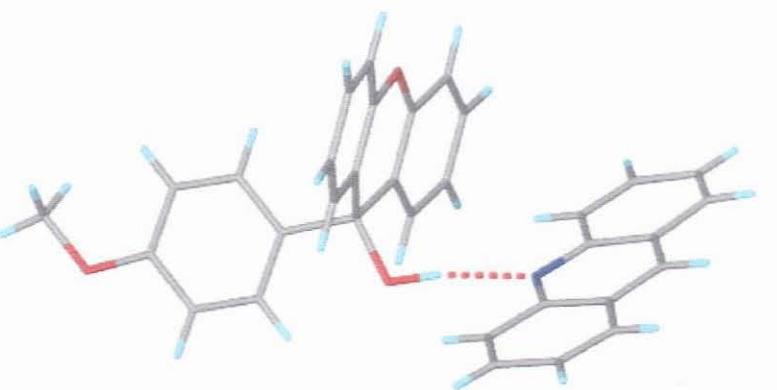

Figure 27 Hydrogen bonding in **A1·ACRI**

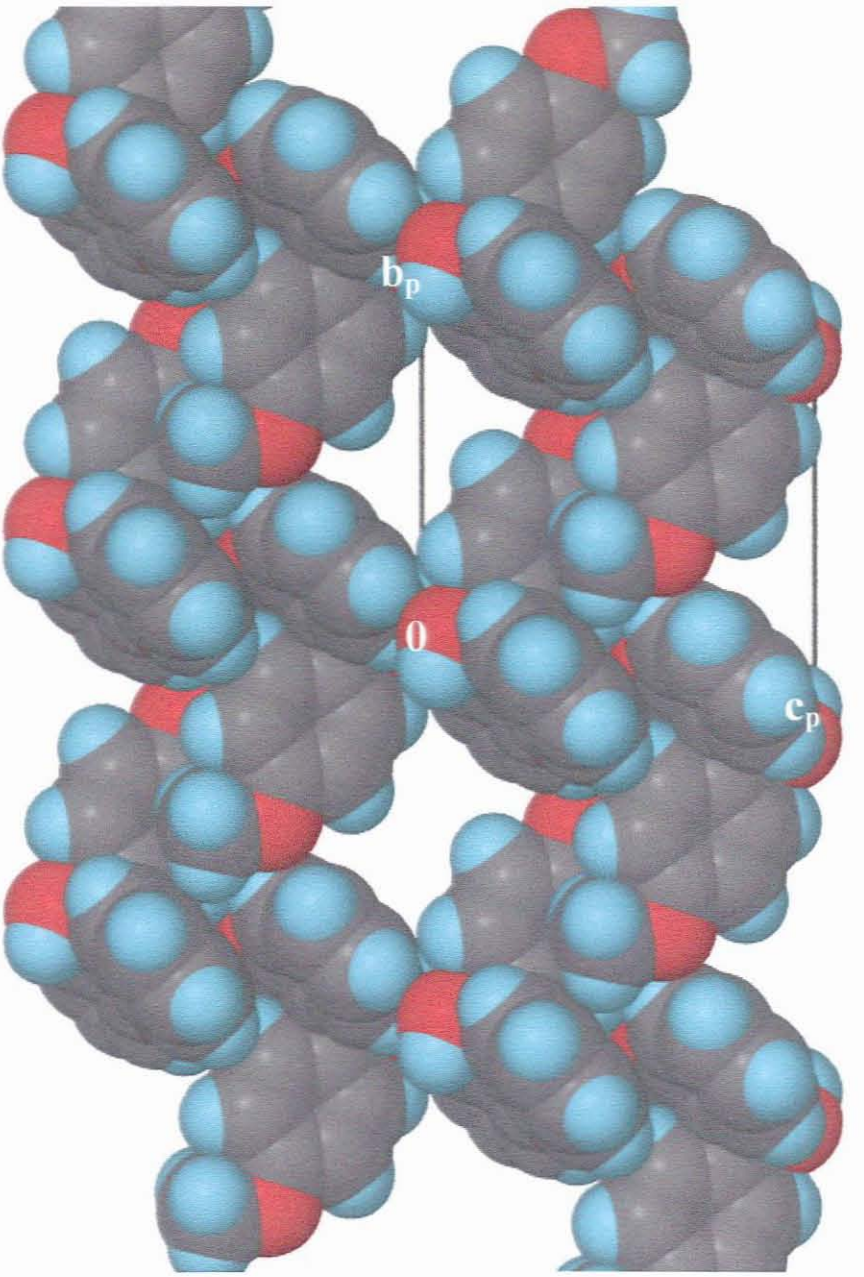

Figure 28 **A1·ACRI** channels down [100] with the guest omitted and host atoms shown in van der Waals radii.

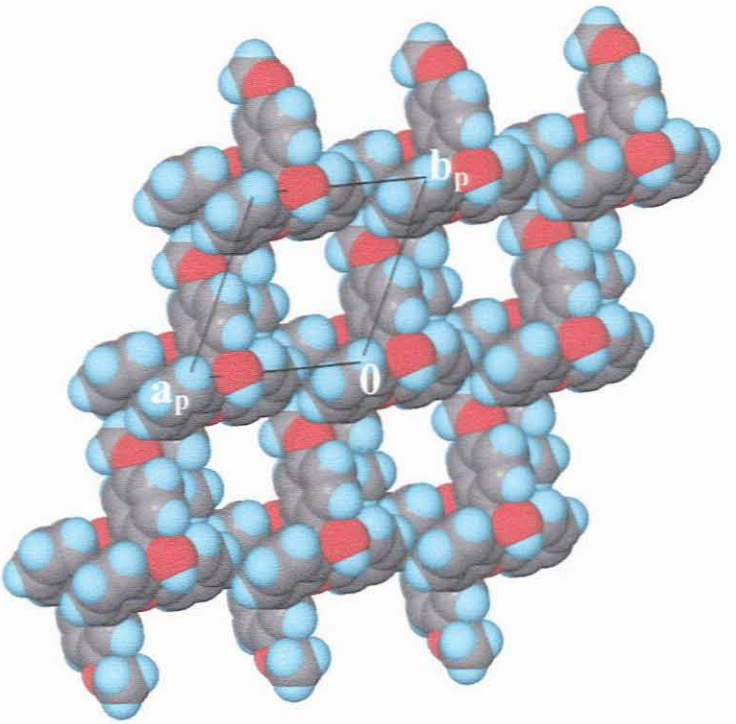

Figure 29 **A1·ACRI** channels down [001] with the guest omitted and host atoms shown in van der Waals radii.

A1·½DABCO

The stoichiometry of the **A1·½DABCO** compound is the same as that of the **A1·½NAPH** and **A1·½HQ** compounds. However the packing is substantially different, in that this compound displays host-guest hydrogen bonding (Fig 30). The **DABCO** guest lies in cavities on a centre of inversion at Wyckoff position *h*, and the ethylenic carbons are all disordered over two positions. The dimensions of the cavity were estimated to be 6.04 Å x 6.67 Å x 6.09 Å. The packing diagram of **A1·½DABCO** down [010] is shown in Figure 31. All hydrogen atoms are omitted for clarity.

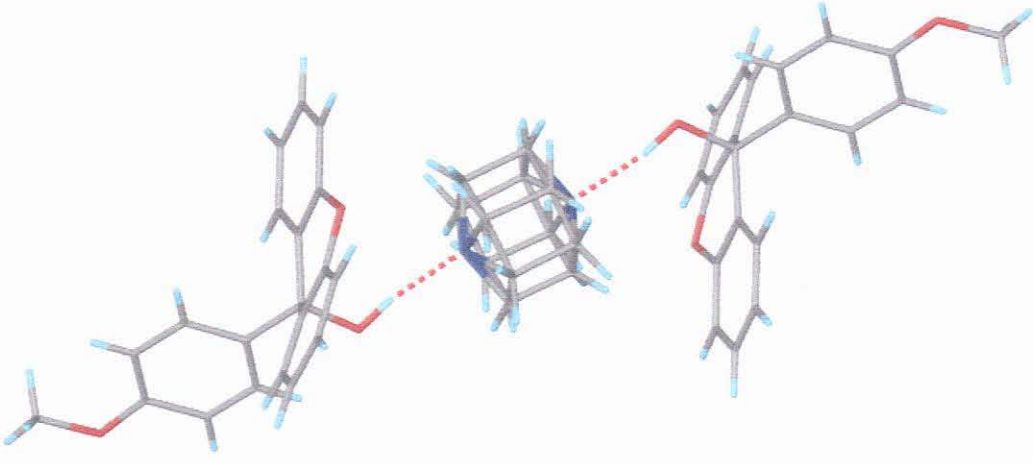

Figure 30 Hydrogen bonding in **A1·½DABCO**.

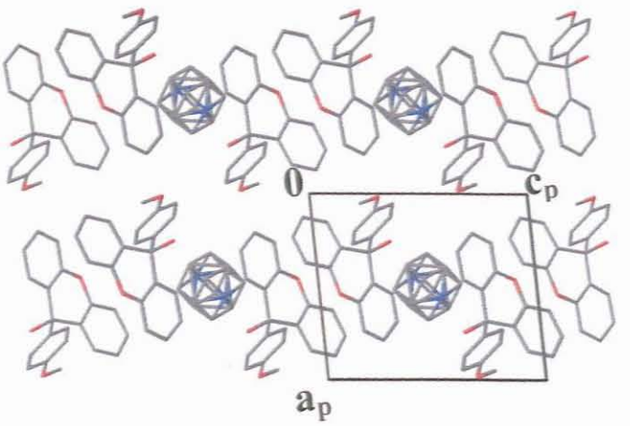

Figure 31 Packing diagram of **A1·½DABCO** down [010].

A1·½BENZAL

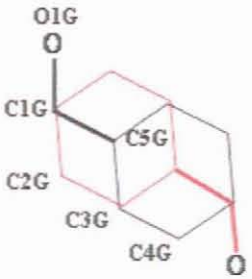

Schematic diagram of benzaldehyde (**BENZAL**) representing the disordered guest.

The structure was solved in the monoclinic space group $P2_1/n$. The host was found in a general position with the guest on a centre of symmetry at Wyckoff position *a*. All the hydrogens were treated in the same manner as was observed for **A1·½NAPH** and **A1·½HQ**. The host molecules form a dimer, (Host)–OH····O–(Host), where the hydroxyl group of one host is hydrogen bonded to the methoxy group of another host. The guest is located in zig – zag channels down [010]. The dimensions of the channels were estimated to be 6.03 Å x 8.34 Å at the wider parts and 4.02 Å x 7.58 Å at the narrower parts.

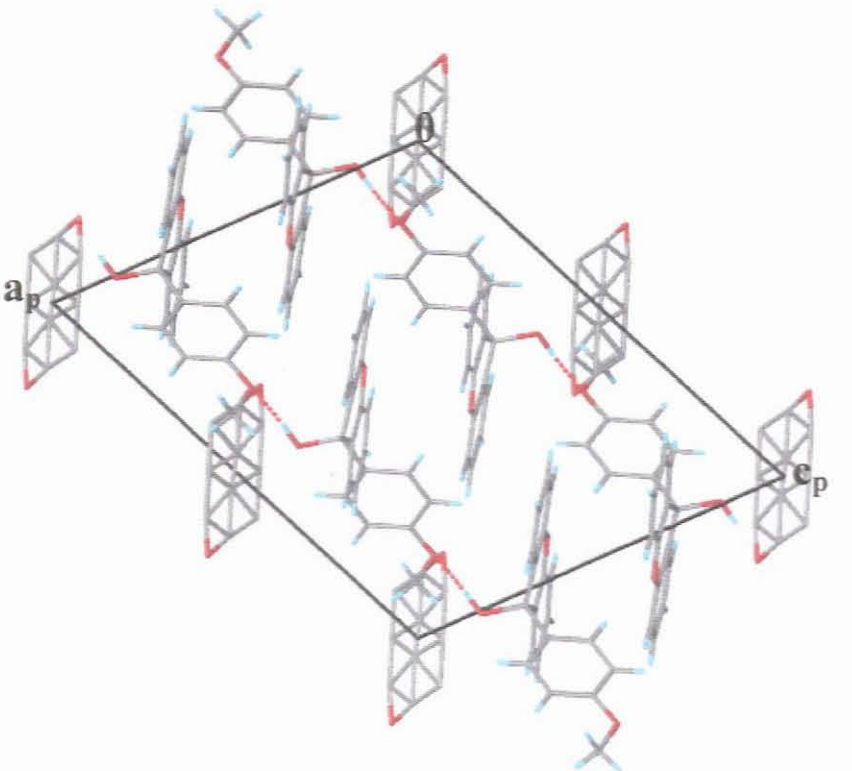

Figure 32 Packing diagram of **A1· ½BENZAL**: Projection viewed down [010]. The H – bonds are plotted as dotted lines.

Discussion

The structures **A1·½NAPH**, **A1·½HQ** and **A1·½BENZAL** are isostructural with respect to the host. The host exhibits the expected packing motif which was previously reported for inclusion compounds between A1 and benzene, toluene, the xylene isomers, [9] aniline, [10] naphthalene, anthracene, phenanthrene, pyrene and *β*-naphthol.[11] The host atoms occupy general positions with the guest molecules located on centres of inversion at Wyckoff position *g* (**NAPH**), *c* (**HQ**) and *a* (**BENZAL**). The host molecules form a centrosymmetric dimer. The host:guest ratios are typically 1:½ with the 1-naphthylamine, 8-hydroxyquinoline and benzaldehyde guests located in channels. Stabilisation of the host network occurs via (Host)–OH···O–(Host) linkages.

For the **A1·½DABCO** structure the host molecule is in a general position with the guest molecule on a centre of inversion at Wyckoff position *h*. This structure displays hydrogen bonding between the host and the guest molecules of the form (Host)–OH···N – (Guest). The stoichiometry is the same as that of the abovementioned compounds with the **DABCO** guest located in a cavity. The **A1·ACRI** structure has a different stoichiometry with a host:guest ratio of 1:1. Also the host molecule is hydrogen bonded to the guest molecule. The acridine guest occupies channels.

PART TWO

RESULTS AND DISCUSSION

The host 9,9'-(ethyne-1,2-diyl)bis(fluoren-9-ol) (**WEB22**) and each of the guest compounds caffeine (**CAF**) and theophylline were dissolved in methanol such that the host: guest ratios were 1:2. The saturated solutions were allowed to crystallise at room temperature. An inclusion compound was formed between the host and caffeine (**WEB22·2CAF).** Theophylline was not included by **WEB22** which formed an inclusion compound with **MeOH** instead (**WEB22·MeOH)**. A mixed crystal, **WEB22·½CAF·MeOH,** was prepared from 50:50 mixtures of caffeine and theophylline with the host **WEB22** using methanol as a mutual solvent. The thermal stabilities and crystal structures will be discussed.

Thermal analysis

We analysed the thermal profiles of the single crystals, grown from solution, of each inclusion compound by DSC. The **WEB22·2CAF** compound yielded a single endotherm corresponding to its melting point (Fig 33). The DSC curve of **WEB22·MeOH** is shown in Fig 34. Thermal analysis results are summarised in Table 7.

Inclusion Compound	WEB22·2CAF	WEB22·MeOH
H:G ratios	1:2	1:1
DSC (T_{on}/K) Endotherm A	455	310
Melting Point of guest (K) Endotherm B	512.7	394.6
Melting Point of host (K) Endotherm C	519.5	505
Endotherm D		466

Table 7 Summary of the DSC results.

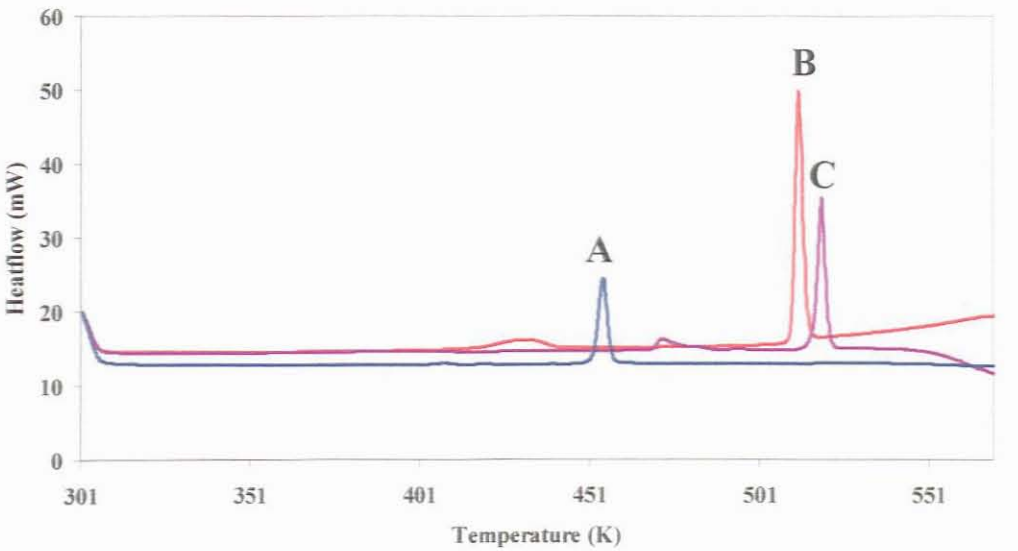

Figure 33 A = melt of **WEB22·2CAF**, B = melt of **CAF** and C = melt of **WEB22**.

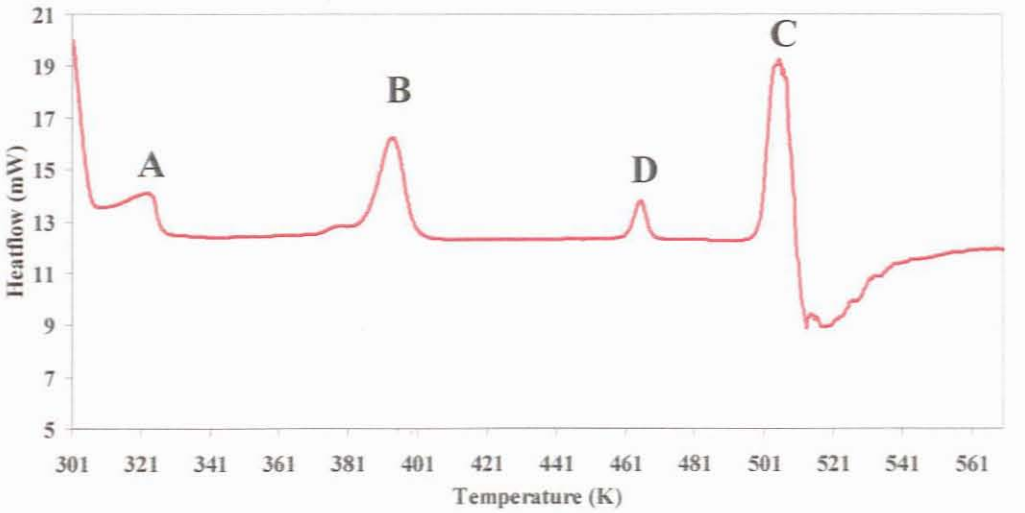

Figure 34 A = loss of surface methanol (**MeOH**), B = loss of included **MeOH**, C = melt and subsequent decomposition of **WEB22** and D = possible phase change.

STRUCTURE DETERMINATION

	WEB22·2CAF	WEB22·MeOH	WEB22·½CAF·MeOH
Compound	½WEB22[a]·$C_8H_9N_4O_2$	2WEB22[a]·$2CH_4O$	2WEB22[a]·$C_8H_9N_4O_2$·$2CH_4O$
M/g mol^{-1}	386.40	836.93	1030.17
T/K	173(2)	173(2)	173(2)
Crystal System	triclinic	triclinic	monoclinic
Space group	$P\bar{1}$	$P\bar{1}$	$P2_1/c$
a/Å	7.2121(14)	9.7592(10)	12.2051(5)
b/Å	9.2782(19)	11.2584(11)	46.8023(19)
c/Å	15.206(3)	20.7854(19)	9.0121(4)
α/°	73.23(3)	97.161(2)	90
β/°	84.20(3)	99.263(2)	91.9650(10)
γ/°	73.39(3)	95.257(2)	90
V/$Å^3$	933.4(3)	2221.8(4)	5144.9(4)
Z	2	2	4
μ/mm^{-1}	0.094	0.080	0.086
F(000)	404	880	2132
Reflections collected/unique	8893/3534	15216/9099	34020/7646
ρ_{calc}/g cm^{-3}	1.375	1.251	1.311
Final R indices [$I > 2\sigma(I)$]	$R_1 = 0.0537$, $wR_2 = 0.1288$	$R_1 = 0.0548$, $wR_2 = 0.1388$	$R_1 = 0.0593$, $wR_2 = 0.1145$
R indices (all data)	$R_1 = 0.0944$, $wR_2 = 0.1501$	$R_1 = 0.0745$, $wR_2 = 0.1524$	$R_1 = 0.0898$, $wR_2 = 0.1249$
Lagest difference peak and hole /e $Å^{-3}$	0.596 and -0.235	0.774 and -0.393	0.391 and -0.307
[a]$C_{28}H_{18}O_2$			

Table 8 Crystal data table

WEB22·2CAF

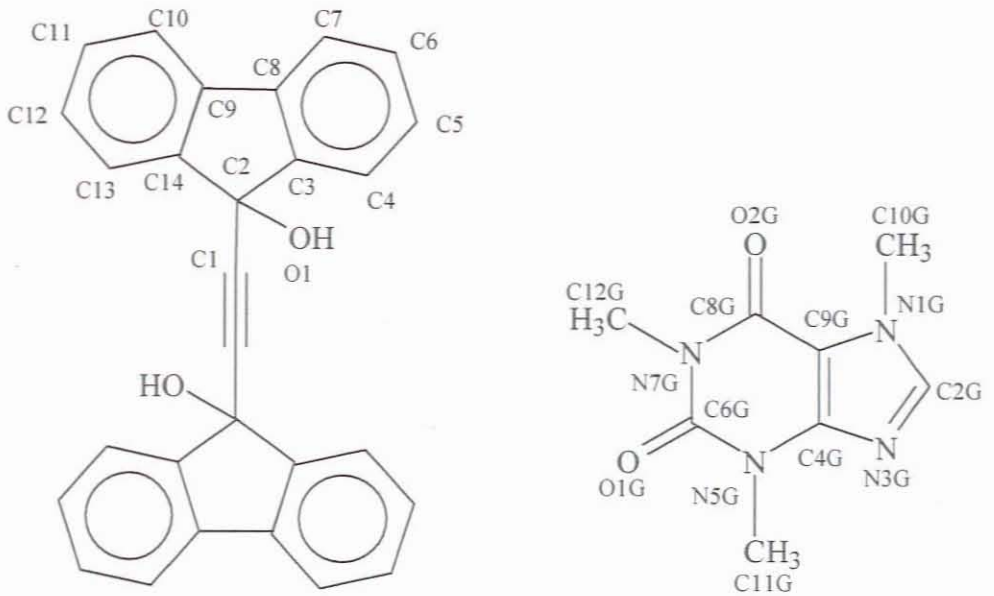

Schematic diagram of the host 9,9'-(ethyne-1,2-diyl)bis(fluoren-9-ol) and the guest caffeine.

The structure was solved in the triclinic space group $P\ \bar{1}$. The host was found on a centre of symmetry at Wyckoff position *d* and the guests were found in general positions (Z = 2). The structure is characterized by alternating layers of the host and guest molecules located on the *ab* plane. The structure is further stabilised by face–to–face π-π stacking interactions between the aromatic rings of adjacent host molecules and between caffeine molecules. There are also C–H···π interactions between host molecules and caffeine guest molecules and between caffeine molecules. The π interactions are summarised in Table 9. The host is on a centre of symmetry and thus the hydroxyl groups are *trans*. The guest molecules lie in large open channels down [100] and [010] as shown in Fig 35 and Fig 36 with the host in van der Waals radii and the guest in stick representation.

The main interaction between the host and guest is a hydrogen bond between the hydroxyl group of the host and the imidazole nitrogen of the caffeine guest; (Host)–OH···N–(Guest). The packing down [100] and [010] is shown in Fig 37 and Fig 38 respectively.

	Distance	**Symmetry operator**	**Angle**
*Cg(C9–C14)···Cg(C3–C8)	approx. 3.936 Å	-x, 2-y, -z	
Cg(N1G–C9G)···*Cg(N5G–C6G)	approx. 3.473 Å	1-x, 1-y, 1-z	
C11G–H11G···Cg(C9–C14)	approx. 3.541 Å		136°
C12G–H12G···Cg(N1G–C9G)	approx. 3.577 Å	-x, 1-y, 1-z	149°
C10G–H10G···Cg(C3–C8)	approx. 4.236 Å	-x, 2-y, 1-z	120°

*Cg = ring centroid

Table 9 π interactions in the **WEB22·2CAF** structure.

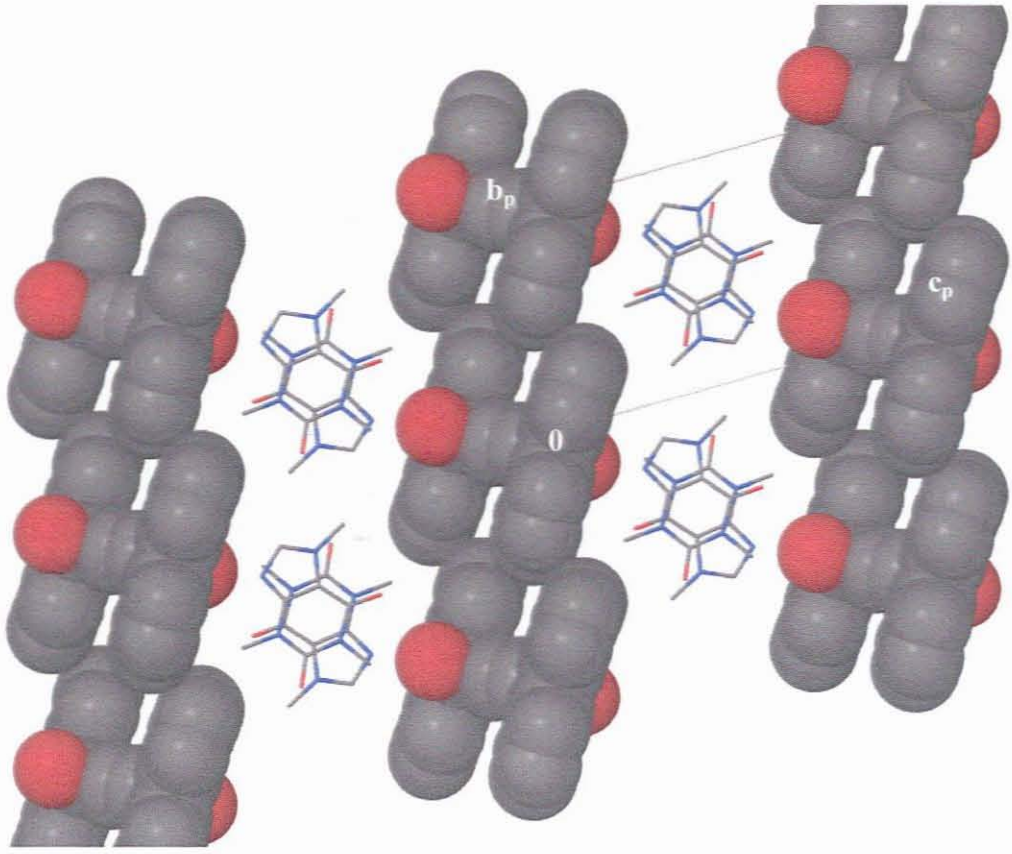

Figure 35 **WEB22·2CAF** channels down [100] with the host in van der Waals radii and the guest in stick representation.

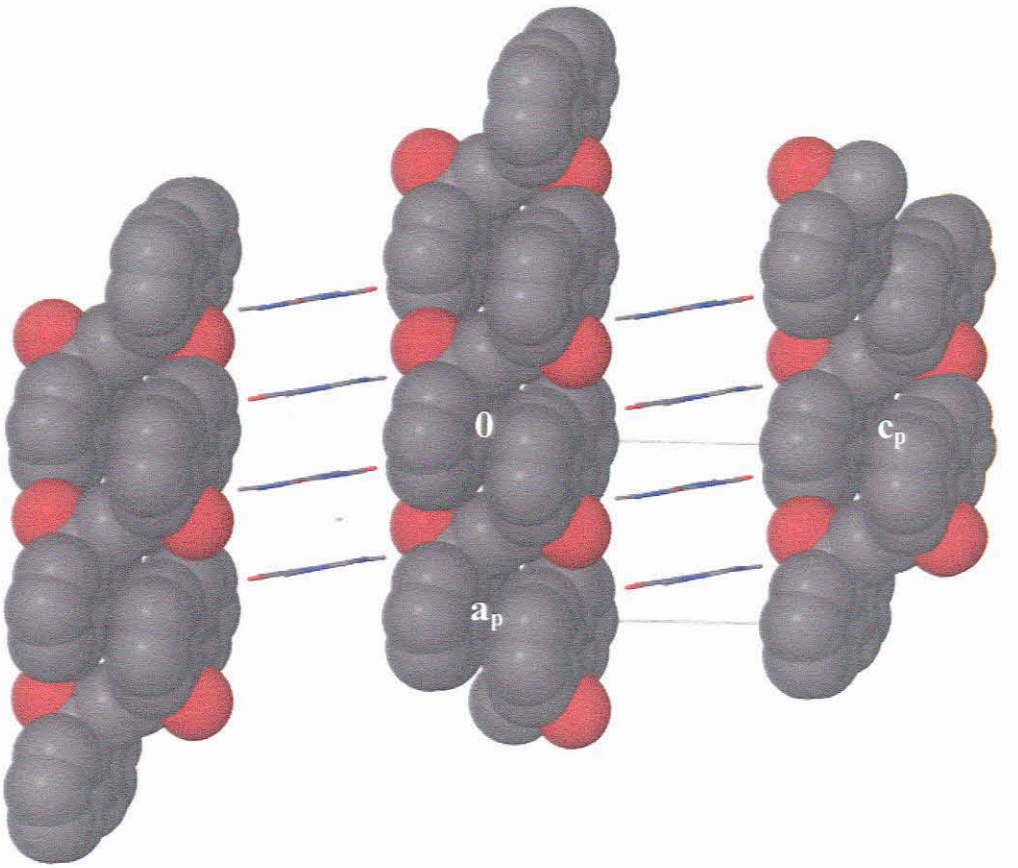

Figure 36 **WEB22·2CAF** channels down [010] with the host in van der Waals radii and the guest in stick representation.

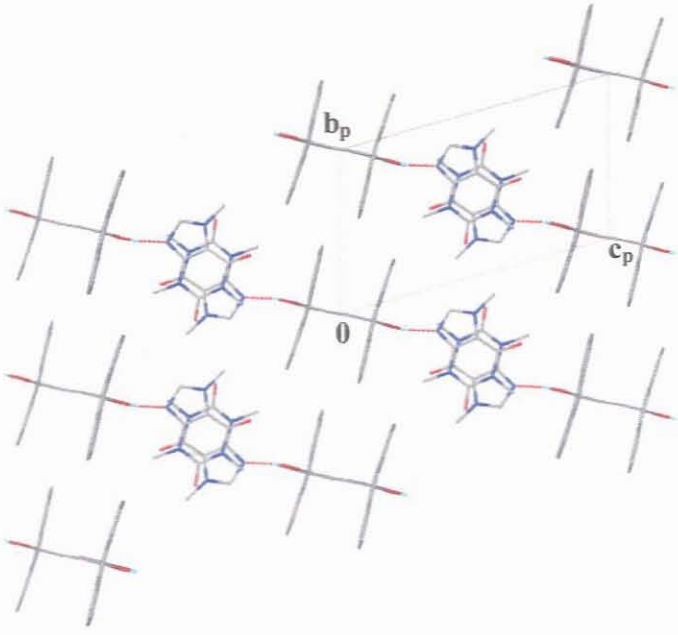

Figure 37 Packing diagram of **WEB22·2CAF**: Projection viewed down [100]. All hydrogen atoms except the hydroxyl hydrogen on the host are omitted. The H – bonds are plotted as dotted lines.

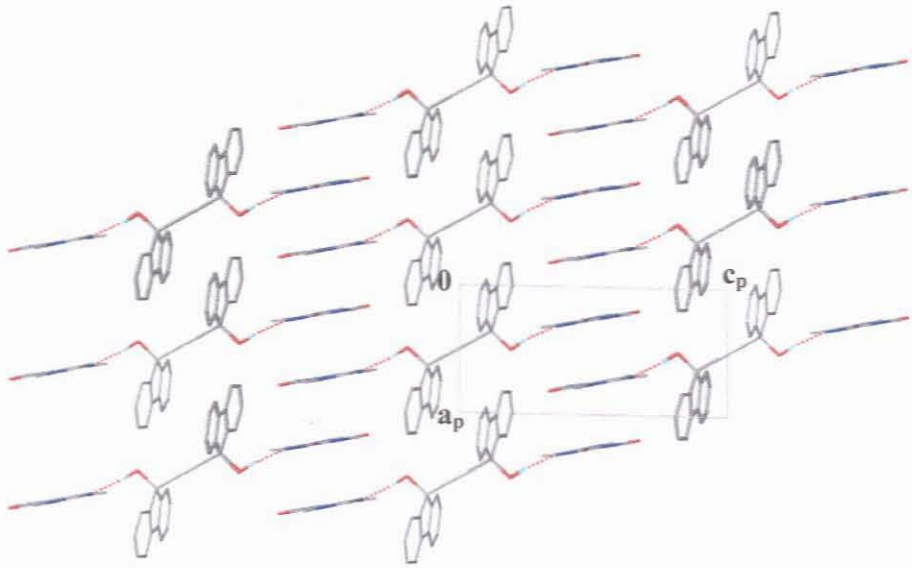

Figure 38 Packing diagram of **WEB22·2CAF**: Projection viewed down [010]. All hydrogen atoms except the hydroxyl hydrogen on the host are omitted. The H – bonds are plotted as dotted lines.

WEB22·MeOH

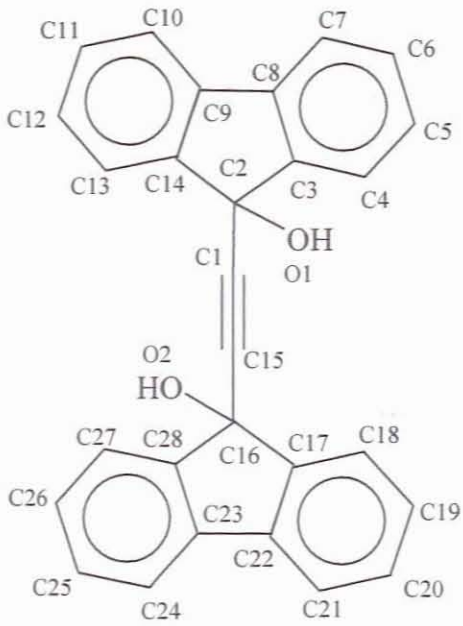

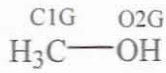

Schematic diagram of the host 9,9'-(ethyne-1,2-diyl)bis(fluoren-9-ol) and the guest methanol. The asymmetric unit contains two host molecules and two guest molecules. The second host molecule and the guest molecule are labelled similarly but with the suffix A.

The structure was solved in the triclinic space group $P\ \bar{1}$. The host and the guest are found in general positions (Z = 2). The hydroxyl group on both host molecules are *cis*. The guests lie in cavities with the dimensions of the cavity estimated to be 4.38 Å x 8.93 Å x 5.09 Å. The main interaction is a three centre bond between two host molecules and one guest molecule that connects the host and the guest molecules into spiral chains parallel to [010]. The structure is further stabilised by face–to–face π-π stacking interactions between the aromatic rings of adjacent host molecules. There are also C–H···π interactions between host molecules and between host molecules and the methanol guest. A summary of π interactions is given in Table 10. The packing diagram with the repeated hydrogen bond motif is shown in Fig 39.

	Distance	Symmetry operator	Angle
Cg(C9A–C14A)···*Cg(C3A–C8A)	approx. 3.791 Å	1-x, 1-y, 1-z	
C10A–H10A···Cg(C17A–C22A)	approx. 3.676 Å	1-x, 1-y, 1-z	139°
O2G–H2G···Cg(C16–C28)	approx. 3.535 Å		130°

*Cg = ring centroid

Table 10 π interactions in the **WEB22·MeOH** structure.

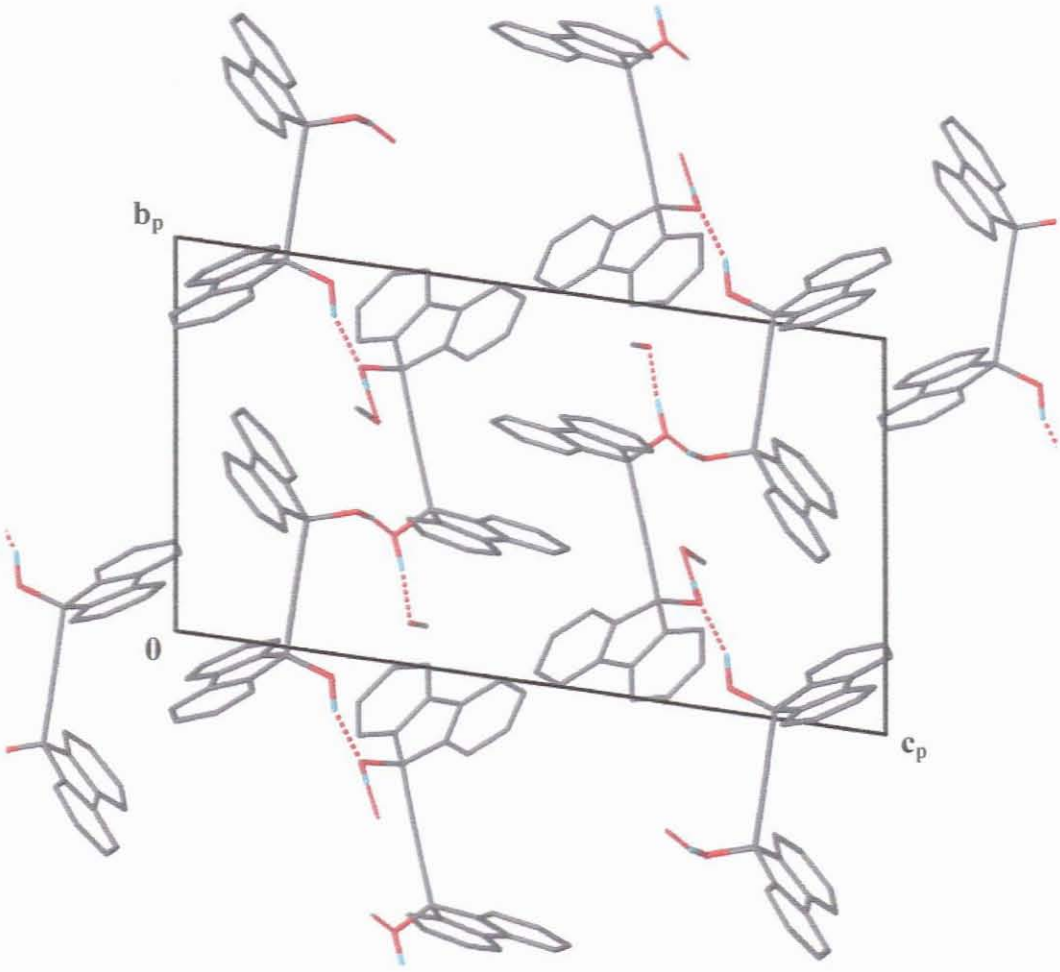

Figure 39 Packing diagram of **WEB22·MeOH**: Projection viewed down [100]. All hydrogen atoms except the hydroxyl hydrogen on the host are omitted. The H – bonds are plotted as dotted lines.

WEB22·½CAF·MeOH

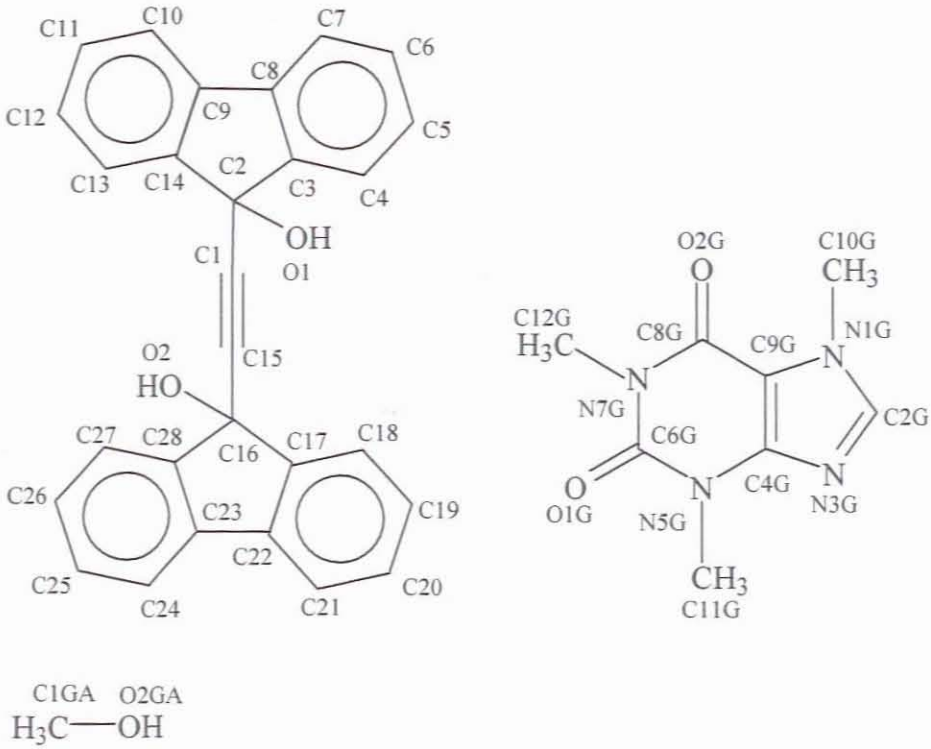

Schematic diagram of the host 9,9'-(ethyne-1,2-diyl)bis(fluoren-9-ol) and the guests caffeine and methanol. The asymmetric unit contains two host molecules, two methanol molecules and one caffeine molecule. The second host molecule is given the suffix A and the second methanol molecule is given the suffix B.

The structure was solved in a monoclinic space group $P2_1/c$. The hydroxyl groups on both host molecules are *cis*. The **MeOH** guest molecules lie in cavities. The structure is characterized by layers of the host and caffeine molecules alternating with **MeOH** guest molecules parallel to [001]. The structure is further stabilised by π interactions (Table 11). A packing diagram indicating the hydrogen bonding is shown in Fig 40.

	Distance	Symmetry operator	Angle
Cg(C17A–C22A)···*Cg(C23A–C28A)	approx. 4.650 Å	-x-1, -y, 2-z	
Cg(C23A–C28A)···*Cg(C17A–C22A)	approx. 4.650 Å	-x-1, -y, 2-z	
C11–H11···*Cg(C17A–C22A)	approx. 4.081 Å	-x, -y, 1-z	141°
C11G–H3G3···*Cg(C22A–C28A)	approx. 3.408 Å	-x, -y, 2-z	107°

*Cg = ring centroid

Table 11 π interaction in **WEB22·½CAF·MeOH** structure.

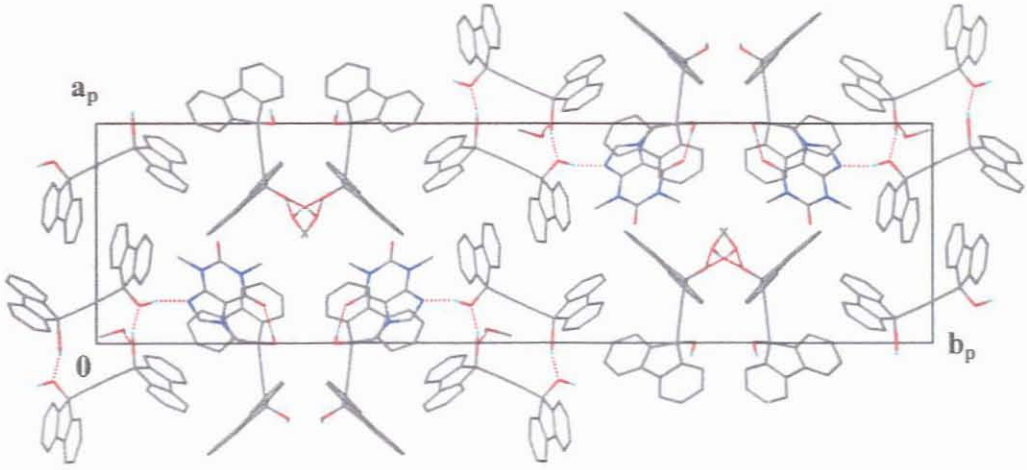

Figure 40 Packing diagram of **WEB22·½CAF·MeOH**: Projection viewed down [001]. All hydrogen atoms except the hydroxyl hydrogen on the host are omitted. The H – bonds are plotted as dotted lines.

	D–H···A	D-H/Å	H···A/Å	D···A/Å	D-H···A/°
WEB22·2CAF	O1-H1···N3G	0.96(1)	1.88(1)	2.823(2)	167(3)
WEB22·MeOH	O1-H1···O2A[a]	1.01(2)	1.72(2)	2.680(2)	158(3)
	O2-H2···O1A[b]	0.98(1)	1.70(1)	2.680(2)	173(3)
	O1A-H1A···O2GA	0.98(1)	1.67(1)	2.617(2)	162(3)
	O2A-H2A···O2G[c]	0.97(1)	1.73(1)	2.706(2)	179(3)
WEB22·CAF·MeOH	O1-H1···O1GB[d]	0.98(1)	1.75(1)	2.696(2)	163(1)
	O2-H2···O2G[e]	0.97(1)	1.81(1)	2.776(2)	178(3)
	O1A-H1A···O2A[f]	0.98(1)	1.72(1)	2.661(2)	161(1)
	O2A-H2A···N3G[g]	0.97(1)	1.80(1)	2.742(3)	162(1)
	O1GA-H1H···O1A	0.753(1)	1.98(1)	2.725(2)	169(1)

[a]1+x, y-1, z ; [b]1+x, y, z ; [c]x-1, y, z ; [d]x, y, 1+z ;[e]1+x, y, z ;[f]-x, -y, 2-z ;[g]-x, -y, 2-z

Table 12 Hydrogen bond data

	D–H···A	D-H/Å	H···A/Å	D···A/Å	D-H···A/°
WEB22·2CAF	O1-H1···N3G	0.96(1)	1.88(1)	2.823(2)	167(3)
WEB22·MeOH	O1-H1···O2A[a]	1.01(2)	1.72(2)	2.680(2)	158(3)
	O2-H2···O1A[b]	0.98(1)	1.70(1)	2.680(2)	173(3)
	O1A-H1A···O2GA	0.98(1)	1.67(1)	2.617(2)	162(3)
	O2A-H2A···O2G[c]	0.97(1)	1.73(1)	2.706(2)	179(3)
WEB22·CAF·MeOH	O1-H1···O1GB[d]	0.98(1)	1.75(1)	2.696(2)	163(1)
	O2-H2···O2G[e]	0.97(1)	1.81(1)	2.776(2)	178(3)
	O1A-H1A···O2A[f]	0.98(1)	1.72(1)	2.661(2)	161(1)
	O2A-H2A···N3G[g]	0.97(1)	1.80(1)	2.742(3)	162(1)
	O1GA-H1H···O1A	0.753(1)	1.98(1)	2.725(2)	169(1)

[a]1+x, y-1, z ; [b]1+x, y, z ; [c]x-1, y, z ; [d]x, y, 1+z ;[e]1+x, y, z ;[f]-x, -y, 2-z ;[g]-x, -y, 2-z

Table 12 Hydrogen bond data

Discussion

All the structures were solved in the triclinic space group $P\bar{1}$ except for **WEB22·½CAF·MeOH** which was solved in the monoclinic space group $P2_1/c$. For **WEB22·MeOH** and **WEB22·½CAF·MeOH** inclusion compounds the hydroxyl groups on the host molecules are *cis*. For the **WEB22·2CAF** structure the host is on a centre of inversion and the hydroxyl groups are subsequently *trans* to one another. All the structures are stabilised by π-π interactions and hydrogen bonding between the host and guest molecules. For the 50:50 mixture of caffeine:theophylline, using methanol as a co-solvent the mixed crystal **WEB22·½CAF·MeOH** was formed. There could be many reasons for the selective inclusion of caffeine over theophylline by the host compound. The methyl group on the imidazole ring of caffeine is electron donating and consequently the nitrogen involved in hydrogen bonding to WEB22 is more electronegative. Thus caffeine has a stronger acceptor nitrogen compared to theophylline. Theophylline was also less soluble in methanol. The bulky methyl group on the imidazole ring of caffeine is also involved in a weak C-H···π contact with the host molecule of approximately 4.236 Å.

REFERENCES

1. Flynn, J. H.; Wall, L. A. *J. Polym. Sci. Part B: Polym. Lett.* **1966**, 4, 323.
2. Faleni, N.; Jacobs, A.; Taljaard, J. H. *J. Chem. Crystallogr.* **2009**, 39, 4, 285.
3. Faleni, N.; Jacobs, A.; Nassimbeni, L. R.; Taljaard, J. H. *Cryst. Growth Des.* **2007**, 7, 6, 1003 – 1006.
4. Sci Finder Scholar (CAS). Advanced Chemistry Development Software V8 - 14.
5. Yvon, K.; Jeitschko, W.; Parthé, E. *J. Appl. Crystallogr.* **1977**, 10, 73-74
6. COLLECT. Data Collection Software. Nonius. Delft. The Netherlands. **1999**.
7. Sheldrick, G. M. SHELXL-97. Program for Crystal Structure Determination. University of Göttingen. Germany. **1997**.
8. Barbour, L. J. LAYER. A computer program for the graphic display of cross sections through a unit cell. *J. Appl. Cryst.* **1999**, 32, 353.
9. Jacobs, A; Nassimbeni, L. R; Su, H; Taljaard, B. *Org. Biomol. Chem.* **2005**, 3, 1319 – 1322.
10. Jacobs, A; Nassimbeni, L. R; Taljaard, B. *Cryst. Growth Des.* **2006**, 7, 731 – 734.
11. Curtis, E.; Nassimbeni, L. R.; Su, H.; Taljaard, J. H. *Cryst. Growth Des.* **2006**, 6, 2716 – 2719.

A1 AND WEB22 HOST CONFORMATIONS

For the host compound A1 five different types of bonds could be classified excluding those involving hydrogen. The different types of bonds are shown in Fig 41. The conformation of the host molecule can be best described by looking at the five unique torsion angles which are demonstrated in Fig 42.

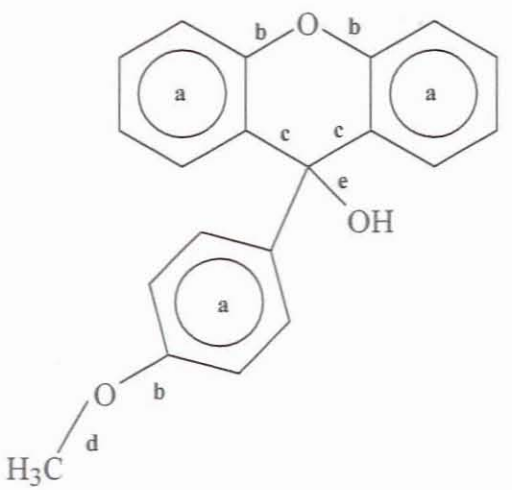

Figure 41 Classification of bonds for **A1**.

Compound	a=C_{ar}–C_{ar} Å	b=C_{ar}–O Å	c=C_{ar}–C_{sp}^3 Å	d=C_{sp}^3–O Å	e=C_{sp}^3–OH Å
A1·½NAPH	1.367(6)	1.384(5)	1.519(6)	1.429(6)	1.453(5)
	1.405(6)	1.400(5)	1.524(5)		
A1·½HQ	1.373(3)	1.373(3)	1.521(3)	1.429(3)	1.45192)
	1.395(3)	1.390(3)	1.528(3)		
A1·ACRI	1.373(2)	1.376(19)	1.524(2)	1.426(19)	1.426(2)
	1.397(2)	1.382(18)			
A1·½DABCO	1376(2)	1.373(16)	1.523(18)	1.424(19)	1.440(15)
	1.398(18)	1.387(15)	1.528(17)		
A1·½BENZAL	1.374(3)	1.374(2)	1.518(2)	1.422(2)	1.446(19)
	1.398(3)	1.380(2)	1.524(2)		

Table 13 Bond length ranges for **A1**.

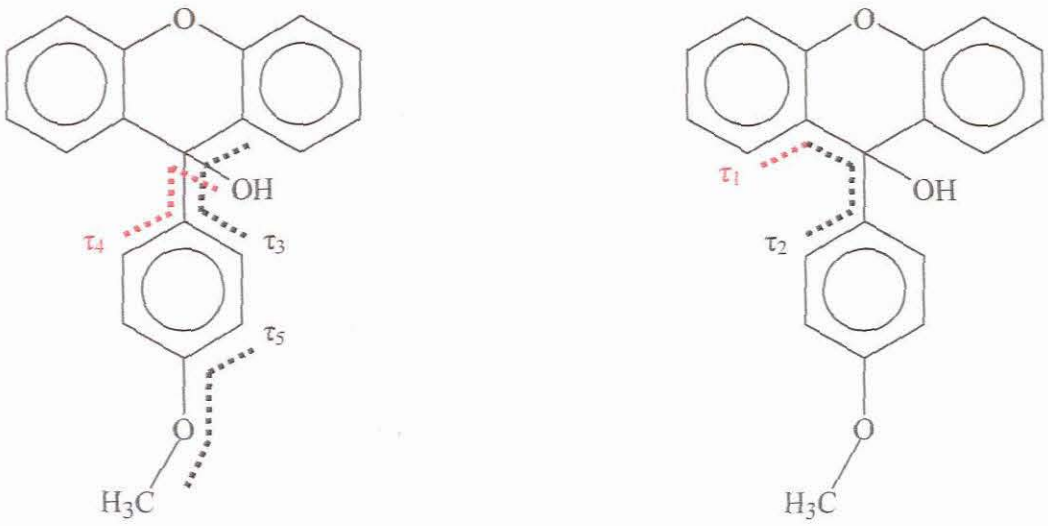

Figure 42 Torsion angles representation.

Torsion angle	A1·½NAPH	A1·½HQ	A1·ACRI	A1·½DABCO	A1·½BENZAL
τ_1	38.3(5)	39.1(3)	71.6(17)	37.5(15)	50.0(2)
τ_2	57.0(5)	66.4(2)	56.1(17)	59.2(15)	69.0(19)
τ_3	114.5(4)	121.4(2)	112.7(15)	118.5(13)	127.2(15)
τ_4	175.6(3)	175.0(17)	176.7(12)	178.8(11)	172.7
τ_5	178.4(4)	179.9(20	175.5(14)	179.4(12)	178.7(17)

Table 14 Torsion angles describing **A1**.

A similar analysis of the bond lengths and torsion angles were completed for **WEB22**.

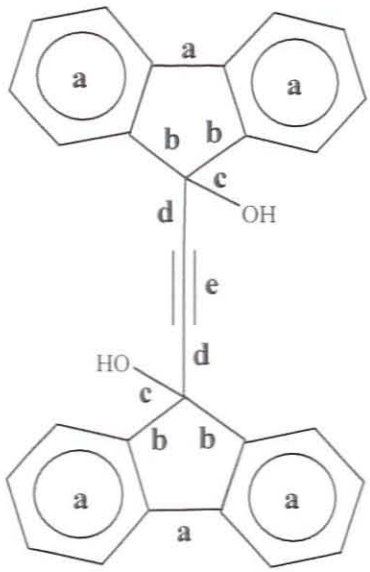

Figure 43 Classification of bonds for **WEB22**.

Compound	a=C_{ar}–C_{ar} Å	b=C_{ar}–$C_{sp}{}^3$ Å	c=$C_{sp}{}^3$–OH Å	d=$C_{sp}{}^3$–C_{sp} Å	e=C_{sp}–C_{sp} Å
WEB22·2CAF	1.373(4)	1.522(4)	1.431(3)	1.475(3)	1.192(5)
	1.469(3)	1.523(4)			
WEB22·MeOH					
HOST 1	1.327(5)	1.517(3)	1.424(2)	1.469(3)	1.192(3)
	1.465(3)	1.538(3)	1.438(2)	1.479(3)	
HOST 1A	1.375(3)	1.521(3)	1.435(2)	1.475(2)	1.193(3)
	1.472(3)	1.528(2)	1.436(2)	1.478(2)	
WEB22·½CAF·MeOH					
HOST 1	1.374(3)	1.527(3)	1.424(3)	1.475(3)	1.188(3)
	1.475(3)	1.535(3)	1.431(3)	1.477(3)	
HOST 1A	1.369(4)	1.519(3)	1.428(3)	1.467(3)	1.197(3)
	1.472(3)	1.528(3)	1.429(3)	1.472(3)	

Table 15 Bond length ranges for **WEB22**.

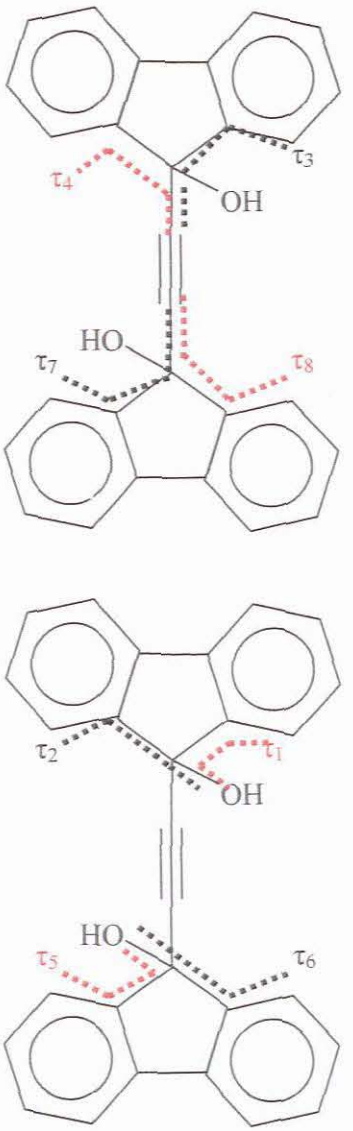

Figure 44 Torsion angles representation.

	τ_1	τ_2	τ_3	τ_4	τ_5	τ_6	τ_7	τ_8
WEB22·2CAF	54.2(3)	-56.4(3)	-66.5(3)	63.1(3)				
WEB22·MeOH								
HOST 1	52.4(3)	-52.3(3)	-66.1(3)	68.1(3)	67.5(2)	-62.8(2)	-56.7(3)	58.5(3)
HOST 1A	-60.1(2)	59.1(2)	59.0(2)	-61.1(2)	57.1(2)	61.4(2)	64.7(3)	-62.4(2)
WEB22·½CAF·MeOH								
HOST 1	67.293)	-70.9(3)	-54.4(3)	55.9(3)	56.8(30	-55.6(3)	-64.2(3)	63.9(3)
HOST 1A	56.2(3)	-66.5(3)	-65.7(3)	59.5(3)	59.2(3)	-60.3(3)	-60.9(3)	59.7(3)

Table 16 Torsion angles describing **WEB22**.

CHAPTER 4

CONCLUSION

CONCLUSION

The compounds 9-(4-methoxyphenyl)-9H-xanthen-9-ol (**A1**) and 9,9'-(ethyne-1,2-diyl)bis(fluoren-9-ol) (**WEB22**) are versatile hosts including a variety of small organic guest molecules. The structures of the host A1 with the guests 1-naphthylamine (**NAPH**), 8-hydroxyquinoline (**HQ**), 1,4-diazabicyclo[2.2.2]octane (**DABCO**), acridine (**ACRI**) and benzaldehyde (**BENZAL**) have been elucidated. They crystallise in two different packing motifs, with **A1·½NAPH**, **A1·½HQ** and **A1·½BENZAL** exhibiting strong host: host hydrogen bond interactions. Host molecules form centrosymmetric dimers of the form (Host)–OH···O–(Host) with the guests occupying centres of inversion. This was previously seen for the inclusion compounds between A1 and benzene, toluene, the xylene isomers, aniline, naphthalene, anthracene, phenanthrene, pyrene, β-naphthol,1,4-dioxane and cyclohexane.

The **A1·½DABCO** and **A1·ACRI** structures, however, exhibit host: guest hydrogen bonding interactions. This behaviour was observed only once before in the case of **A1·DMF**. The host – guest compounds **A1·½NAPH**, **A1·½HQ**, **A1·½DABCO** and **A1·ACRI** were also formed by grinding of the two solids. The kinetics of the reactions were monitored by powder X-ray diffraction and followed the first order rate law $\ln(1-\alpha) = -kt$ where α is the extent of reaction. Non – isothermal kinetics of desolvation were performed for **A1·½BENZAL** and they gave activation energies in the range 74 kJ mol^{-1} – 86 kJ mol^{-1}.

Host – guest hydrogen bonding was observed for the inclusion compounds of **WEB22** involving the guests caffeine (**CAF**) and methanol (**MeOH**). A mixed crystal was

obtained from the host with the two guests caffeine and methanol. All these inclusion compounds are governed by hydrogen bonding networks and π-π interactions. The WEB22 caffeine-theophylline system highlights the importance of subtle changes in guest functionality on selectivity. Caffeine has a stronger nitrogen acceptor compared to theophylline which renders it more attractive to the hydroxyl groups of WEB22. The methanol co-solvent in this system also plays a role as methanol competes with caffeine and is selectively included over theophylline.